Hybrid inorganic–organic materials: a new family in condensed matter physics

2008 J. Phys.: Condens. Matter 20 083202

(http://iopscience.iop.org/0953-8984/20/8/083202)

IOP Publishing Journal of Physics: Condensed Matter

J. Phys.: Condens. Matter **20** (2008) 083202 (21pp) doi:10.1088/0953-8984/20/8/083202

TOPICAL REVIEW

Hybrid inorganic–organic materials: a new family in condensed matter physics

C N R Rao[1], A K Cheetham[2] and A Thirumurugan[1]

[1] Chemistry and Physics of Materials Unit, Jawaharlal Nehru Centre for Advanced Scientific Research, Jakkur PO, Bangalore 560 064, India
[2] Department of Materials Science and Metallurgy, University of Cambridge, Pembroke Street, Cambridge CB2 3QZ, UK

E-mail: cnrrao@jncasr.ac.in and akc30@cam.ac.uk

Received 20 October 2007, in final form 20 November 2007
Published 1 February 2008
Online at stacks.iop.org/JPhysCM/20/083202

Abstract

We review some recent trends in an emerging field at the interface between classical inorganic and organic materials. Hybrid inorganic–organic framework materials are crystalline systems in which both inorganic and organic structural elements co-exist within a single phase. Much of the focus in this area during the last few years has been on porous hybrid frameworks, which are of interest for potential applications in catalysis, separations and sensors. The primary focus of our overview is on properties that traditionally lie in the domain of condensed matter physics: magnetism, optical, electronic and dielectric properties. We show that these materials exhibit a rich diversity of behavior in these areas and present some exciting opportunities for the physics community. We also present a short summary of some of the properties found in porous materials.

(Some figures in this article are in colour only in the electronic version)

Contents

1. Introduction

Hybrid inorganic–organic framework compounds constitute an important class of materials that have been studied extensively over the last few years due to their potential applications in catalysis, gas separation and storage. Other properties which draw attention to these materials include magnetic, optical and electronic properties [1]. It is necessary to understand where hybrid materials belong relative to conventional coordination compounds. Starting with the pioneering work of Werner on coordination compounds, for which he was awarded the Nobel Prize in Chemistry in 1913, the field of coordination polymers has turned out to be rich and varied. Coordination compounds with infinite structures, the so-called coordination polymers, have been intensively studied, in particular compounds with backbones constructed from metal ions as nodes and ligands as linkers. The term, 'coordination polymers' appeared in the early 1960s, and the area was first reviewed in 1964 [2].

A vast range of coordination polymers or supramolecular architectures with one-, two-and three-dimensional structures have been discovered. Examples of one-dimensional (1D) coordination polymers are relatively common in the early literature, even though they were not recognized at the time as part of a vast and remarkable family of materials. Examples include porphyrin coordination polymers with interesting

magnetic properties, first discovered by Basolo and co-workers in the 1970s and characterized by x-ray diffraction at a later date [3, 4]. Early examples of nanoporous 3D coordination polymers can be found in the work of Gravereau, Garnier and Hardy in the late 1970s, in which zeolitic materials with ion-exchange properties were made by linking hexacyanoferrate units with tetrahedrally coordinated Zn^{2+} cations [5]. The components of coordination polymers are connected through coordination bonds, which are weaker in energy than the strong Si/Al–O bonds that sustain the structures of zeolites. Thus, coordination polymers have rather poorer thermal stability, though they are sufficiently robust for many applications, especially in systems with extended inorganic connectivity, e.g. metal–oxygen–metal bonds.

The development of hybrid inorganic–organic framework materials may be traced back to a strategy that was originally used to increase the interlayer spacing in layered compounds, the most notable being the layered zirconium phosphonates [6, 7]. However, there was relatively little interest in hybrid materials until the 1990s, when several groups, particularly those of Robson, Hoffman and Yaghi, recognized that rigid, polyfunctional organic molecules could be used to bridge metal cations or clusters into extended arrays. Robson published a landmark paper in 1990 [8], laying the groundwork for an important part of the field of crystal engineering—the science of predicting basic networks with potentially useful characteristics and then using appropriate molecular building blocks to synthesize them [9–11]. For the synthesis of porous materials, networks are often envisioned where rigid organic molecules and metal atoms or clusters replace bonds and atoms in classical inorganic structures [12]. Since then, several groups have focused on synthesizing and characterizing novel hybrid metal oxides based on carboxylates [13–18].

Hybrid inorganic–organic framework materials are defined as compounds that contain both inorganic and organic moieties as integral parts of a network with infinite bonding connectivity in at least one dimension [18]. This definition excludes systems that are molecular or oligomeric. Most of the known hybrid frameworks may be divided into two categories. The coordination polymers, or metal organic frameworks (MOFs) as they are also known (especially when they are porous), can be defined as extended arrays composed of isolated metal atoms or clusters that are linked by multifunctional organic ligands, L; these are based upon M–L–M connectivity. Second, there are systems that contain extended arrays of inorganic connectivity, referred to as extended inorganic hybrids. At present, the vast majority of known materials in this area are based upon oxygen bridges. These hybrid metal oxides, which contain infinite metal–oxygen–metal (M–O–M) arrays as a part of their structures, represent a sub-group of a larger class in which there is extended M–X–M bonding via other atoms such as Cl, N or S.

2. Classification

In table 1, we show the range of possibilities in terms of M–ligand–M, (O^m, where m represents the dimensionality of the ligand bridging) or extended inorganic dimensionalities (I^n, where n represents the dimensionality of the inorganic connectivity). The overall dimensionality of the structure is then represented with the notation I^nO^m. The entire family of molecular coordination compounds is contained within a single box (I^0O^0) in table 1 (i.e. both M–L–M (m) and inorganic connectivity (n) = 0). The remaining three boxes in the first column represent the coordination polymers with overall dimensionality 1–3. The three boxes in the second column represent hybrid compounds with 1D inorganic connectivity (I^1) and with an overall dimensionality between 1 and 3. The two boxes in the third column represent hybrid compounds with two-dimensional (2D) inorganic connectivity (I^2) and with the overall dimensionality of 2 or 3. The first box in the fourth column represents a rare class of hybrid compound (I^3O^0) with a three-dimensional (3D) inorganic connectivity (I^3) and with the overall dimensionality of 3. There are examples of all of these classes of hybrid materials (table 2 and figure 1) [19–26]. Currently there are no examples

Table 1. Classification of inorganic–organic hybrid framework solids.

Metal–organic–metal connectivity, O^n (n = 0–3) \ Dimensionality of inorganic connectivity, I^n (n = 0–3)	0	1	2	3
0	Molecular complexes I^0O^0	Hybrid inorg. chains I^1O^0	Hybrid inorg. layers I^2O^0	3-D Inorg. hybrids I^3O^0
1	Chain coordination polymers I^0O^1	Mixed inorg.–organic layers I^1O^1	Mixed inorg.–organic 3-D framework I^2O^1	—
2	Layered coordination polymers I^0O^2	Mixed inorg.–organic 3-D framework I^1O^2	—	—
3	3-D Coordination polymers I^0O^3	—	—	—

Table 2. Examples of the different classes of inorganic–organic hybrid compounds.

I^nO^m	Formula	Figure	Ref
I^0O^0	$[Mn(H_2O)(1,3\text{-CHDC})(1,10\text{-phen})]$	1(a)	[19]
I^0O^1	$[Mn_3(1,3\text{-CHDC})_3(1,10\text{-phen})_2]\cdot 4H_2O$	1(b)	[19]
I^0O^2	$[Cd(H_2O)_2(1,3\text{-CHDC})]\cdot 2H_2O$	1(c)	[19]
I^0O^3	$Zn_4O(1,4\text{-BDC})_3$, terephthalate	1(d)	[20]
I^1O^0	$[Nd_2(H_2O)2(C_{14}H_8O_4)_3]$, diphenate	1(e)	[21]
I^1O^1	$[Cd(H_2O)_2(1,3\text{-BDC})]$, isophthalate	1(f)	[22]
I^1O^2	$[La_3(1,4\text{-HCHDC})_2(1,4\text{CHDC})_5(H_2O)_2]\cdot H_2O$	1(g)	[23]
I^2O^0	$[Cd(1,2\text{-CHDC})]$	1(h)	[19]
I^2O^1	$Co_2(H_2O)_2(O_3P(CH_2)_2PO_3)$, phosphonate	1(i)	[24]
I^3O^0	$[Ni_7(OH)_2(C_4H_4O_4)_6(H_2O)_2\cdot 2H_2O]$, succinate	1(j)	[25]
I^3O^0	$[Cd(C_3H_2O_4)(H_2O)]\cdot H_2O$, malonate	1(k)	[26]

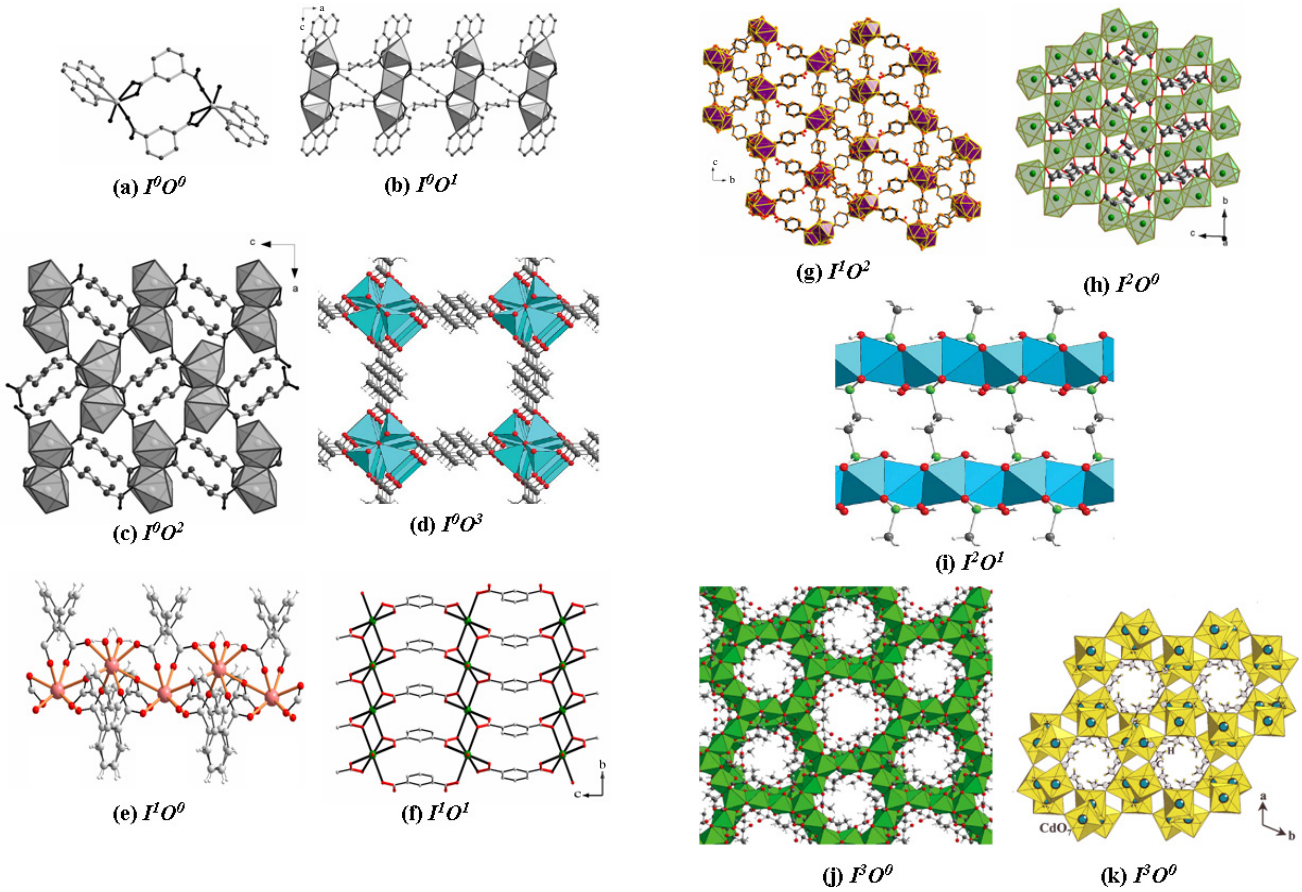

Figure 1. (a) A molecular Mn-1,3-cyclohexanedicarboxylate, $[Mn(H_2O)(1,3\text{-CHDC})(1,10\text{-phen})]$, of the type I^0O^0, (b) a 1D Mn-1,3-cyclohexanedicarboxylate, $[Mn_3(1,3\text{-CHDC})_3(1,10\text{-phen})_2]\cdot 4H_2O$, of the type I^0O^1, (c) a 2D Cd-1,3-cyclohexanedicarboxylate, $[Cd(H_2O)_2(1,3\text{-CHDC})]\cdot 2H_2O$, of the type I^0O^2, (d) a 3D Zn-1,4-benzenedicarboxylate, $Zn_4O(1,4\text{-BDC})_2.x(\text{solvent})$, of the type I^0O^3, (e) a 1D Nd-diphenate, $[Nd_2(H_2O)2(C_{14}H_8O_4)_3]$, of the type I^1O^0, (f) a 2D Cd-1,3-benzenedicarboxylate, $[Cd(H_2O)_2(1,3\text{-BDC})]$, of the type I^1O^1, (g) a 3D La-1,4-cyclohexanedicarboxylate, $[La_3(1,4\text{-HCHDC})_2(1,4\text{-CHDC})_5(H_2O)_2]\cdot H_2O$, of the type I^1O^2. Copyright Wiley-VCH Verlag GmbH & Co. KGaA. Reproduced with permission from [23], (h) a 2D Cd-1,3-cyclohexanedicarboxylate, $[Cd(1,2\text{-CHDC})]$, of the type I^2O^0, (i) a 3D Co-diphosphonate, $Co_2(H_2O)_2(O_3P(CH_2)_2PO_3)$, of the type I^2O^1, reprinted with permission from [24]. Copyright 2007 American Chemical Society, (j) a 3D Ni-succinate, $[Ni_7(OH)_2(C_4H_4O_4)_6(H_2O)_2\cdot 2H_2O]$, of the type I^3O^0, and (k) a 3D Cd-Malonate, $[Cd(C_3H_2O_4)(H_2O)]\cdot H_2O$, of the type I^3O^0.

for the empty boxes in the bottom right part of the table 1 except one, a manganese camphorate, which has (I^3O^1) connectivity with 3D achiral inorganic connectivity and 1D chiral organic connectivity [27]. Hybrid compounds with zero inorganic connectivity are coordination polymers, which can be represented as ${}_xI^0O^m$ where x represents the nuclearity of the metal site. For compounds with isolated metal sites, $x = 1$ and for cluster metal sites, $x > 1$.

3. Synthetic methods

The synthesis of crystalline hybrid framework materials while preventing the precipitation of amorphous solid remains a challenge, and novel methodologies are being investigated to access them. Synthetic strategies [28] for the preparation of crystalline hybrid materials may be categorized as follows. (i) Coordination-directed assembly of metal complexes by multifunctional organic ligands, or the bottom-up method. The structural integrity of the building units is maintained throughout the reactions which allow their use as modules in the assembly of extended structures. (ii) pH-controlled condensation of metal hydroxide or hydrate units to form extended M–O–M linkages. (iii) Combination of the above two, i.e. partial condensation of oxide components intercepted by coordination and linking by multidentate ligands. The extent of oxide bridging and structure condensation increases with reaction temperature.

The above strategies are realized in terms of two important techniques of crystallization, namely (i) diffusion based crystallization and (ii) hydro/solvo/ionothermal methods. Good quality single crystals can be generally obtained by layered diffusion, which is preferred for coordination polymers of desired stoichiometry. Hybrid compounds with extended inorganic connectivity are generally prepared by hydro/solvo thermal methods to overcome the differing solubilities of the organic as well as inorganic components and to enhance the degree of condensation [29]. Ionothermal methods have been employed recently for the synthesis of the hybrid compounds, wherein ionic liquids are used as solvents [30, 31].

The use of hydrothermal methods and relatively high reaction temperatures (up to, say, 250 °C) generally produces

compounds with increased M–O–M connectivity. For example, five different cobalt succinate structures could be synthesized using identical starting mixtures by varying only the temperature [32]. The extent of oxide bridging and structure condensation increases with reaction temperature. In a more comprehensive study of the cobalt succinate system by high throughput experimentation, the trends as a function of pH and time were also examined [33]. It was found that extended inorganic hybrid structures are also favored at high pH, where the formation of M–O–M linkages arise due to the elimination of water or hydroxide groups by condensation reactions. The evolution of reaction products as a function of time, however, showed relatively few changes, supporting the idea that thermodynamic factors are often very important in hybrid synthesis.

Hybrid compounds have also been synthesized by microwave-assisted solvothermal synthesis [34–37]. An advantage in this method is that local superheating of the solvent (or the organic ligand, L) can lead to hot spots that nucleate crystal growth all over the system. More seeds lead to faster growth and higher yields. Once the seeds start to grow, the available reactants get quickly depleted. The size of the crystals can, therefore, be varied by adjusting the reactant concentration. The ability of the microwave technique to control the nucleation process leads to a narrow size distribution, because all of the crystals are nucleated at once. It also allows new types of frameworks to be discovered readily since the growth process is not depending on nucleation on the walls or dust particles. Since the hot spots in microwave-assisted reactions with certain organic solvents are known to produce excessive pressure and heat, extra care must be taken. Since ionic liquids with high polarizability and ionic conductivity exhibit excellent microwave absorption behavior, they are used as solvents for microwave-assisted ionothermal synthesis of hybrid compounds [31].

Another recent method is the high throughput hydrothermal method, which involves systematic studies of the roles of various synthesis parameters and this helps for a quick investigation [32].

4. Magnetic properties

The magnetic properties of hybrid inorganic–organic compounds, in which extended inorganic networks or local paramagnetic centers (mostly of transition metal and lanthanide ions) are linked by diamagnetic linkers that can efficiently mediate magnetic exchange, have evoked considerable interest. The mode of linkage and the dimensionality of the inorganic sub network, along with the size, geometry, chemical functionality and various coordinating modes of the linkers, provide excellent means of controlling and modulating the magnetic properties in these solids.

A variety of magnetic properties have been found with hybrid materials, of particular interest being those with ferromagnetic (FM) properties (table 3). For example, a chiral 3D nickel glutarate, $[Ni_{20}(H_2O)_8(C_5H_6O_4)_{20}\cdot 40H_2O]$ shows a pure co-operative ferromagnetic behavior ($T_c \approx 4$ K), without any spin frustration [38]. The I^3O^0 type 3D connectivity in this compound arises as the helices of edge-sharing octahedra connected to four parallel neighboring ones through a nickel octahedron. The oxide framework is walled by two independent glutarate anions (figure 2). The low T_c value is due to the weakness of the ferromagnetic interaction for a Ni–O–Ni bridge angle significantly larger than 90°.

A cobalt 1,4-cyclohexane dicarboxylate, $[Co_5(OH)_8(CHDC)\cdot 4H_2O]$, has a T_c of 60 K, a temperature that is among the highest observed in this class of compounds [39]. Its structure is based on metal–hydroxide octahedral–tetrahedral layers pillared by dicarboxylate ions (I^2O^1 type). These layers are closely related to the brucite type but with one out of every four octahedra removed and replaced by two tetrahedra above and below the layer (figure 3). Each tetrahedron shares three corners with octahedra and the cobalt coordination is completed by unidentate carboxylate groups of the CHDC pillars. A 3D framework is thus formed that contains channels filled with water. The dehydration–rehydration process is reversible, thereby conferring to this hybrid some porous properties. Removal of the water molecules leads to a shift of the layers combined with a tilt and a rotation of the organic moieties and a shortening of the interlayer space of about 1 Å.

From *cis, cis*-cyclohexane-1,3,5-tricarboxylic acid (H_3CTC), 3D hybrid compounds with both cobalt and nickel, $[M_3(H_2O)_4(\textit{trans}\text{-}CTC)_2\cdot 5H_2O]$, have been synthesized [41]. The structure comprises a lozenge-shaped tunnel topology with inorganic chains connected by the organic moiety. The four oxide chains in this compound are all connected through two central tricarboxylates into a 3D structure. The chains are constructed by dimers of edge-sharing octahedra, connected through a third octahedron which shares its *trans* vertices with two neighboring dimers through a μ_2-OH_2. These compounds behave as short-range coupled low-dimensional chains with a tendency to ferrimagnetic alignment of the moments for the cobalt compound and ferromagnetic for the nickel compound.

The cobalt succinate, $[Co_5(OH)_2(C_4H_4O_4)_4]$, exhibiting ferrimagnetic interactions, is a 2D metal oxide framework pillared by the succinate moiety into a 3D network (I^2O^1) [42]. It is constructed from zig-zag layers of edge-sharing cobalt octahedra that generate pentamers of octahedra and 12-membered ring cavities (figure 4). The succinate moieties act as bridges between the sheets. This compound exhibits ferrimagnetic behavior below 10 K, which results from (i) antiferromagnetic couplings within the pentamers, (ii) ferromagnetic coupling between the pentamers to avoid the compensation of the moments, which implies a ferromagnetic interaction in agreement with the largest superexchange angles of the structure and (iii) ferromagnetic coupling between the layers. According to Goodenough, d^7–d^7 superexchange 180° interactions are always antiferromagnetic, the 90° ones can be either antiferromagnetic (e_g–p–t_{2g}) or ferromagnetic (e_g–p_σ–p_σ–e_g). Another ferrimagnetic cobalt succinate, $[Co_4(OH)_2(H_2O)_2(C_4H_4O_4)_3\cdot 2H_2O]$, of the type I^2O^0, contains a 2D Co–O–Co network with 14-membered ring windows and can be described as parallel 'helicoidal' chains of octahedra connected by tetrameric units of co-planar octahedra through edge sharing. Succinate anions link the cobalt atoms within each layer [43]. The occluded and

Table 3. Magnetic properties of representative inorganic–organic hybrid compounds.

S. no	Formula	I^nO^m	Description of properties	Figure	Reference
(a) Ferromagnetic (FM)					
1	Glutarate $[Ni_{20}(H_2O)_8(C_5H_6O_4)_{20}\cdot 40H_2O]$	I^3O^0	$T_c \approx 4$ K	2	[38]
2	1,4-cyclohexane dicarboxylate $[Co_5(OH)_8(CHDC)\cdot 4H_2O]$	I^2O^1	$T_c \approx 60$ K	3	[39]
3	Succinate $[Ln_2(C_4H_4O_4)_3(H_2O)_2]\cdot 0.5H_2O$ Ln = Gd, Dy	I^1O^2	Super exchange interaction	—	[40]
4	cyclohexane-1,3,5-tricarboxylate $[Ni_3(H_2O)_4(CTC)_2\cdot 5H_2O]$	I^1O^2	Dominant AFM interaction till 190 K, FM-LRO at lower temp	—	[41]
(b) Ferrimagnetic (FiM)					
1	Succinate $[Co_5(OH)_2(C_4H_4O_4)_4]$	I^2O^1	$T_N \approx 10$ K	4	[42]
2	Succinate $[Co_4(OH)_2(H_2O)_2(C_4H_4O_4)_3\cdot 2H_2O]$	I^2O^0	$T_N \approx 10$ K	—	[43]
3	Fumarate $[Ni_3(OH)_2(H_2O)_4(C_4H_2O_4)_2\cdot 2H_2O]$	I^1O^2	$T_N \approx 20$ K	5	[44]
4	3,4-pyridinecarboxylate $[Mn_3(OH)_2(3,4\text{-pyda})2(H_2O)_2]$	I^1O^2	$T_N \approx 7$ K	—	[45]
(c) Metamagnetic (MM)					
1	Terephthalate $[Co_2(OH)_2(1,4\text{-BDC})]$	I^2O^1	Intralayer FM and interlayer AFM ($T_N \approx 48$ K)	6	[46]
2	Azide $[Cu_2(N_3)_4(L)]$, (L = 1,2-bis(tetrazol-1-yl)ethane, 1,4-bis-(tetrazol-1-yl)butane)	I^2O^1	Short range FM and interlayer AFM	—	[47]
3	1,4-naphthalenedicarboxylate $[Co(C_{12}H_6O_4)]$	I^1O^2	$T_C \approx 5.5$ K, Intrachain FM and interchain AFM	7	[48]
d) Canted antiferromagnetic (CAFM)					
1	Terephthalate $[Co_2(OH)_2(1,4\text{-BDC})]$	I^2O^1	$T < 45$ K	6	[46]
2	Terephthalate $V_2^{IV}O_2F_2\{O_2C\text{–}C_6H_4\text{–}CO_2\}$	I^2O^1	$T < 20$ K	—	[49]
3	2,5-pyridinedicarboxylate $[Co_3(NC_5H_3(CO2)_2)(OH)_2(H_2O)_2]$	I^1O^2	$T < 30$ K	8	[50]
e) Antiferromagnetic (AFM)					
1	Succinate $[Co_6(OH)_2(C_4H_4O_4)5\cdot H_2O]$	I^2O^1	$T_N \approx 26$ K	—	[51]
2	Ethylenediphosphonate $M_2^{II}(H_2O)_2(O_3P(CH_2)_2PO_3)$, M = Co and Ni	I^2O^1	$T_N \approx 7$ K, M = Co $T_N \approx 13$ K, M = Ni	1(i)	[24]
3	Terephthalate $V(OH)\{1,4\text{-BDC}\}\cdot x(1,4\text{-}H_2BDC)$	I^1O^2	$T_N \approx 95$ K	—	[51]
4	Terephthalate $Fe_2O\{O_2C\text{–}CH_3\}_2\{1,4\text{-BDC}\}\cdot 2CH_3OH$	I^1O^2	$T_N \approx 5$ K	—	[53]

coordinated water can be removed from this compound in a reversible process. This compound is ferrimagnetic below 10 K due to antiferromagnetic coupling within the helicoidal chain and ferromagnetic coupling in the tetramer. It is well known that in 90° superexchange interactions, small variations of the angle around the superexchange 'blank angle' can invert the sign of the coupling constant (90°–100°, depending on the nature of the 3d transition metal cation). Large superexchange angles lead to antiferromagnetic interactions while weaker ones induce ferromagnetic coupling. In this case, the blank angle is in the 98°–99° range.

The nickel fumarate, $[Ni_3(OH)_2(H_2O)_4(C_4H_2O_4)_2\cdot 2H_2O]$, consists of a metal oxide chain built from trimers consisting of two edge-sharing octahedra linked by a μ_3-OH to a vertex of a third one. The chains are connected by fumarate ions to form a 3D framework of the type I^1O^2 (figure 5) [44]. This compound behaves as a ferrimagnet, $T < 20$ K, with a spontaneous magnetization below 6 K. A possible spin–orbit

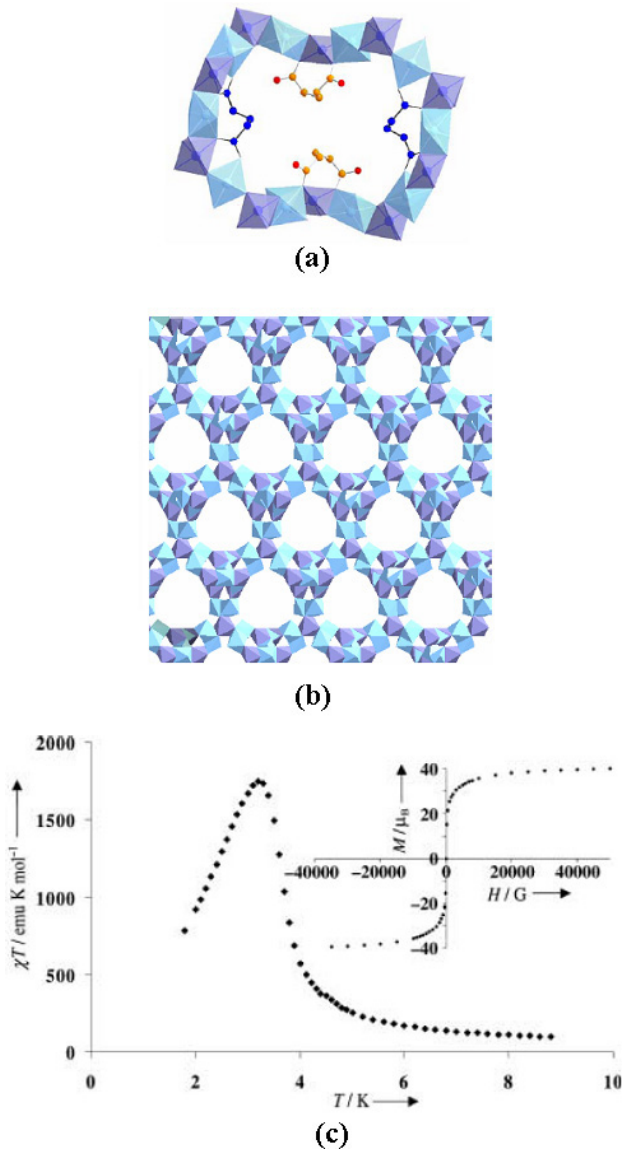

Figure 2. (a) Polyhedral view of a corrugated 20-membered ring with two independent glutarate ions, (b) a view of the nickel oxide tunnels down [111] in 3D glutarate $[Ni_{20}(H_2O)_8(C_5H_6O_4)_{20}\cdot 40H_2O]$ and (c) thermal dependence of the χT product. The inset shows the magnetization versus the applied magnetic field at 2 K. Copyright Wiley-VCH Verlag GmbH & Co. KGaA. Reproduced with permission from [38].

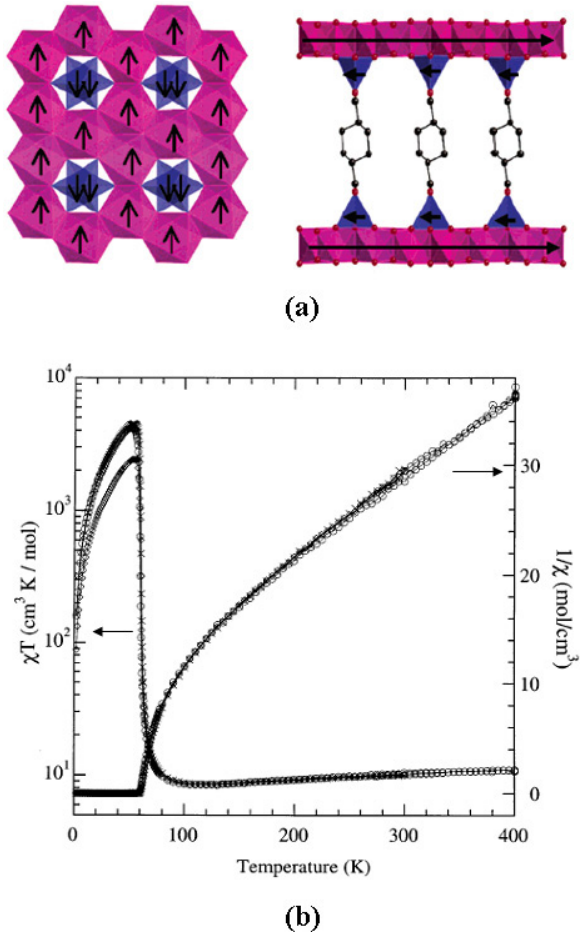

Figure 3. (a) Diagrammatic representation of the proposed magnetic ordering at the tetrahedral and octahedral cobalt(II) sites in 1,4-cyclohexane dicarboxylate, $[Co_5(OH)_8(1,4\text{-CHDC})\cdot 4H_2O]$ and (b) temperature dependence of the inverse magnetic susceptibility and of the product of susceptibility and temperature: virgin (O), dehydrated (X) and rehydrated (◊). Reprinted with permission from [39]. Copyright 2003 American Chemical Society.

coupling along with a small spin frustration due to additional exchange pathways through fumarate ions explain the 3D co-operative magnetization.

A 3D cobalt terephthalate, $[Co_2(OH)_2(1,4\text{-BDC})]$, of the I^2O^1 type is built up from inorganic layers where two types of parallel tilted chains of edge-sharing octahedra are linked by OH bridges [46]. The layers are then connected together through terephthalate linkers into a 3D architecture (figure 6). Magnetic studies show that the intralayer exchange interaction between Co(II) ions is ferromagnetic, but the whole system orders antiferromagnetically at 48 K with a metamagnetic (MM) transition above a threshold field of 0.2 T. The existence of conjugated π electrons in the terephthalate bridges explains the antiferromagnetic interactions between the layers. Below 45 K, the compound exhibits canted antiferromagnetism associated with a non-collinear orientation of the moments between the layers. The magnetization loop shows a large coercive field of 5.9 T at 4.2 K, which must be related to extremely large single-ion anisotropy on the Co sites. The copper analog of the above cobalt terephthalate, however, exhibits ferromagnetic coupling through the terephthalate bridge between the ferromagnetic sheets with in-plane interaction $J = +5.5$ K, probably due to Jahn–Teller effects.

A simple cobalt 1,4-naphthalenedicarboxylate, $[Co(C_{12}H_6O_4)]$, of the I^1O^2 type consists of chains of metal octahedral connected by the organic moiety into a 3D framework. The chain is zig-zag and constructed from edge-sharing cobalt octahedra (figure 7) [48]. The compound exhibits metamagnetic behavior ($T_C = 5.5$ K) with strong ferromagnetic intrachain interactions and antiferromagnetic interchain interactions.

An interesting cobalt 2,5-pyridinecarboxylate, $[Co_3(NC_5H_3(CO2)_2)(OH)_2(H_2O)_2]$, with a 3D structure of the I^1O^2 type

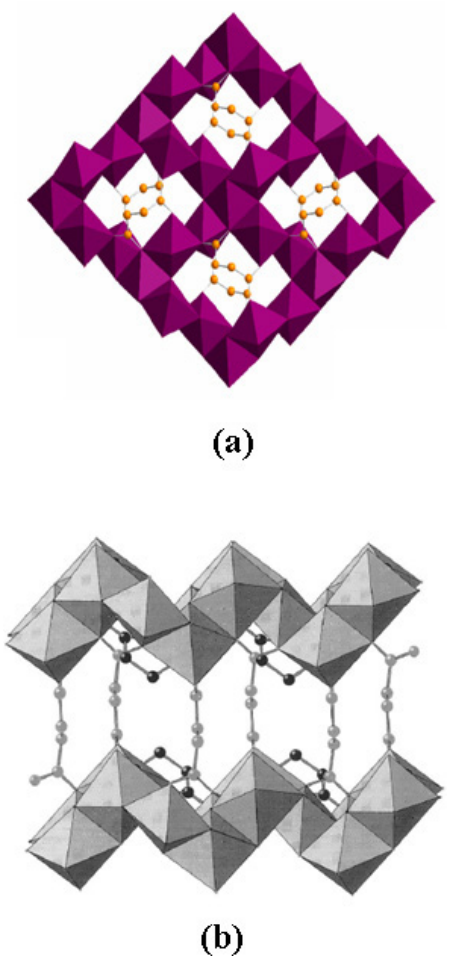

Figure 4. (a) View of the 2D inorganic layer in a 3D cobalt succinate $[Co_5(OH)_2(C_4H_4O_4)_4]$ and (b) a view of the 3D structure where 2D layers are connected by succinate anions. From [42]. Reproduced by permission of The Royal Society of Chemistry.

consists of chains of CoO_x ($x = 5$ and 6) polyhedra with three different geometries [50]. These chains of hydroxide-bridged scalene triangles (not equilateral) share edges and vertices and are further connected by the ligand into a 3D structure (figure 8). In small fields below 30 K the susceptibility increases as the measuring field decreases, which is consistent with canted antiferromagnetism producing a small but significant coercive field of 200 G. Three different areas of bistability (A—less than 500 G, B—5000–12 000 G and C—above 18 000 G) have been observed due to the field-induced reorientation of spins. The magnetization saturates at slightly more than 18 000 G cm^3 mol^{-1} compared with 62077 G cm^3 mol^{-1} calculated for ferromagnetic alignment, which suggests a spin structure in which 1/3 of the Co(II) ions are uncompensated (e.g. as shown in figure 8(C)). Magnetic bistability may be observed in materials with ferromagnetic, ferrimagnetic, canted antiferromagnetic or metamagnetic spin arrangements, but it is rare to observe more than one area of bistability in a single material. This behavior is ascribed to the competing superexchange and dipolar exchange pathways, the different g values associated with different coordination geometries and the structural anisotropy of the material.

Table 4. Magnetic properties of organically templated Kagome compounds.

TM ion	Spin (S)	Magnetic properties
Mn^{2+}	5/2	AFM interaction
Fe^{3+}	5/2	Magnetic frustration and AFM interaction
Co^{2+}	3/2	Magnetic frustration and AFM ordering
Fe^{2+}	2	Ferromagnetic interaction
Ni^{2+}	1	Canted AFM interaction

A large number of hybrid compounds with I^1O^x frameworks exhibit AFM interactions (table 3e) [24, 51–53], especially compounds of the type I^1O^1 and I^1O^2. Also compounds with I^0 (zero inorganic connectivity, first column in table 1) generally show AFM interactions. Compounds with FM interactions are of greater interest, but good examples of hybrid compounds with strong FM interactions are yet to be discovered. Such compounds, especially if they are nanoporous, would be valuable since they might be able to separate nitrogen and oxygen, making use of the paramagnetism of molecular oxygen. Hybrid frameworks with homo-or hetero-metallic clusters linked by various types of organic connectors would be of interest as model compounds to understand low-dimensional magnetism and frustrated magnetic systems.

Several transition metal compounds possessing the Kagome structure, wherein hexagonal bronze type inorganic layers are templated by organic amines, have been synthesized and characterized in the last few years [54, 55]. An example of the amine templated metal sulfate is shown in (figure 9). One would expect all Kagome compounds to exhibit magnetic frustration, characteristic of a triangular lattice [56]. Kagome compounds containing Mn^{2+}, Co^{2+}, Fe^{2+}, Fe^{3+} and Ni^{2+} exhibit different magnetic properties, as shown in table 4. We readily see that Kagome compounds comprising transition metal ions with non-integral spins such as Mn^{2+}, Co^{2+} and Fe^{3+} exhibit magnetic frustration or low-temperature antiferromagnetism. Magnetic frustration is minimized in compounds containing transition metal ions with integral spins such as Ni^{2+} and Fe^{2+}. Furthermore they also show evidence for ferromagnetic interactions. Theoretical investigations suggest that the spin magnitude of the transition metal ion plays a crucial role in determining the magnetic frustration and related properties of the Kagome compounds [57].

Clearly, the magnetic properties of hybrid materials offer much scope for further investigations. Some of the challenges would be to synthesize high T_c ferromagnets, ferromagnets with channels and those showing magnetoresistance.

5. Optical properties

Optical properties of hybrid framework materials are of interest partly because of their greater stability compared with molecular materials, since adequate thermal, chemical and optical stability is a pre-requisite for commercial applications. Porous, chiral and magnetic hybrids exhibiting photo- and electroluminescence (table 5) and nonlinear optical activity have evoked interest.

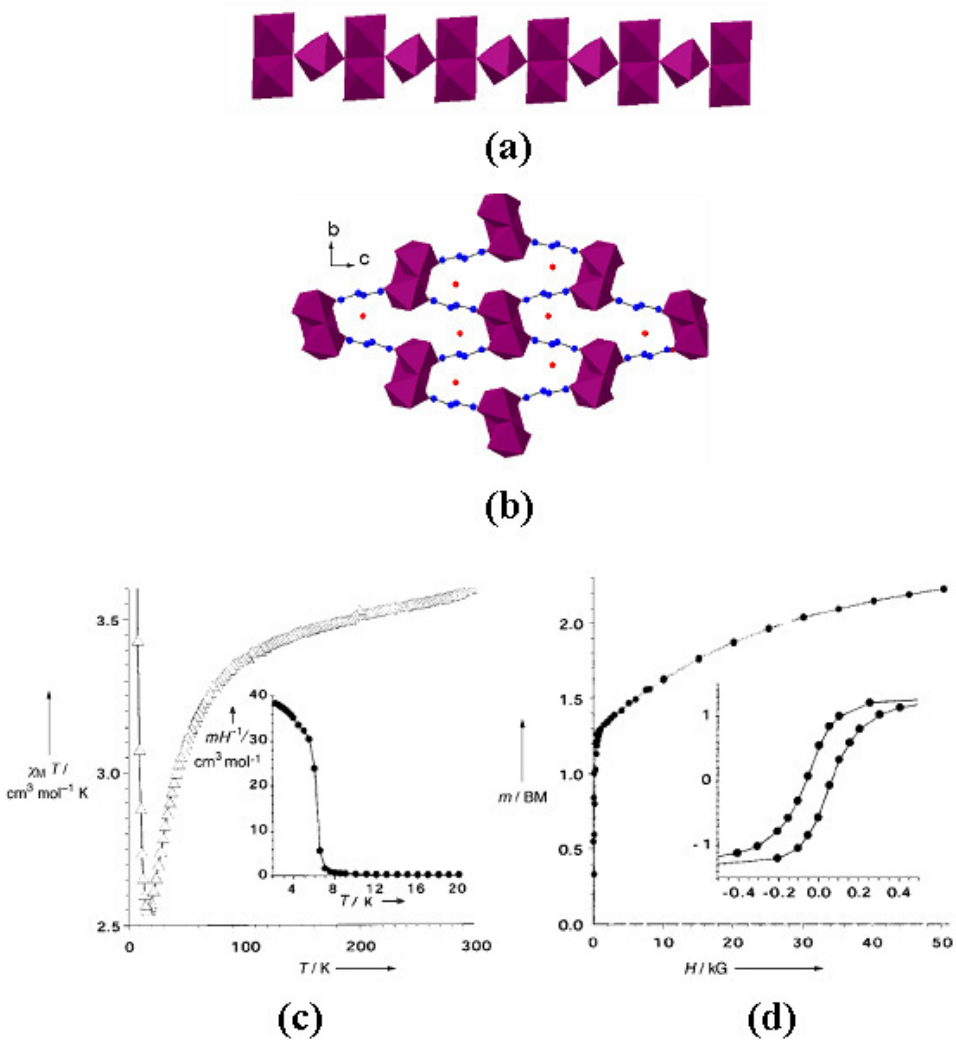

Figure 5. (a) The 1D nickel oxide chain in 3D fumarate, $[Ni_3(OH)_2(H_2O)_4(C_4H_2O_4)_2{\cdot}2H_2O]$, (b) view of the 3D structure where 1D chains are connected by fumarate anions, (c) plot of $\chi_M T$ versus T. Inset shows a field-cooled magnetization curve (under an applied magnetic field $H = 100$ G) showing ferromagnetic order at 6 K and (d) magnetization curve at 2 K. Inset shows hysteresis loop at 2 K with decreasing H first. Copyright Wiley-VCH Verlag GmbH & Co. KGaA. Reproduced with permission from [44].

5.1. Photoluminescence

Many hybrid frameworks that exhibit photoluminescence (PL) do so as a result of intraligand transitions or charge transfer (metal to ligand (MLCT) or ligand to metal (LMCT)) excitations. Another important source is metal-centered PL, especially with hybrids containing rare earth ions. Ligand-centered emissions may be significantly enhanced due to the rigidity of the framework, which reduces energy losses due to radiationless decay (σ–σ^* or π–π^*) compared to free molecules. The lifetime of the emission can be tuned by introducing heavy metals like lead with increased spin–orbit coupling, thereby reducing the radiative lifetime of triplets resulting in room temperature phosphorescence. A range of examples is given in table 5.

The 2D cadmium phthalate, [Cd(1,2-BDC)(H_2O)], of the type I^2O^0, exhibits strong fluorescent emission in the solid state at room temperature. The structure consists of a honeycomb inorganic Cd–O–Cd layer with edge and corner shared (CdO_7) pentagonal bipyramids. The short π–π^* luminescence ($\lambda_{max} = 407$ nm, $\tau = 0.021$ ms) was assigned to intraligand fluorescent emission [58]. A 3D cadmium oxalate, $[Cd_2(C_2O_4)(OH)_2]$, of the type I^2O^1, with infinite cadmium hydroxide corrugated layers connected through oxalate units, exhibits strong fluorescent emission bands in the solid state at room temperature at 380 and 400 nm ($\lambda_{ex} = 340$ nm). These are attributed to a $\pi^* \rightarrow n$ intraligand transition (figure 10) [59]. It also exhibits another strong emission at 432 nm (λex $= 360$ nm), which was assigned to ligand-to-metal charge transfer (LMCT).

A 3D porous, $[Cd_3L_6](BF_4)_2$-$(SiF_6)(OH)_2{\cdot}13.5H_2O$, where L = 2,6-di-(4-triazolyl)pyridine, exhibits tunable emission between UV and visible wavelengths (figure 11) [60]. The compound and a series of its dehydrated derivatives display intense luminescence with emission maxima ranging from the UV (380 nm—intraligand fluorescence) to the visible region (438 nm—LMCT). With rehydration, the fluorescent emissions shift back from visible light (438 nm) to the UV region (382 nm). This phenomenon was attributed to weak

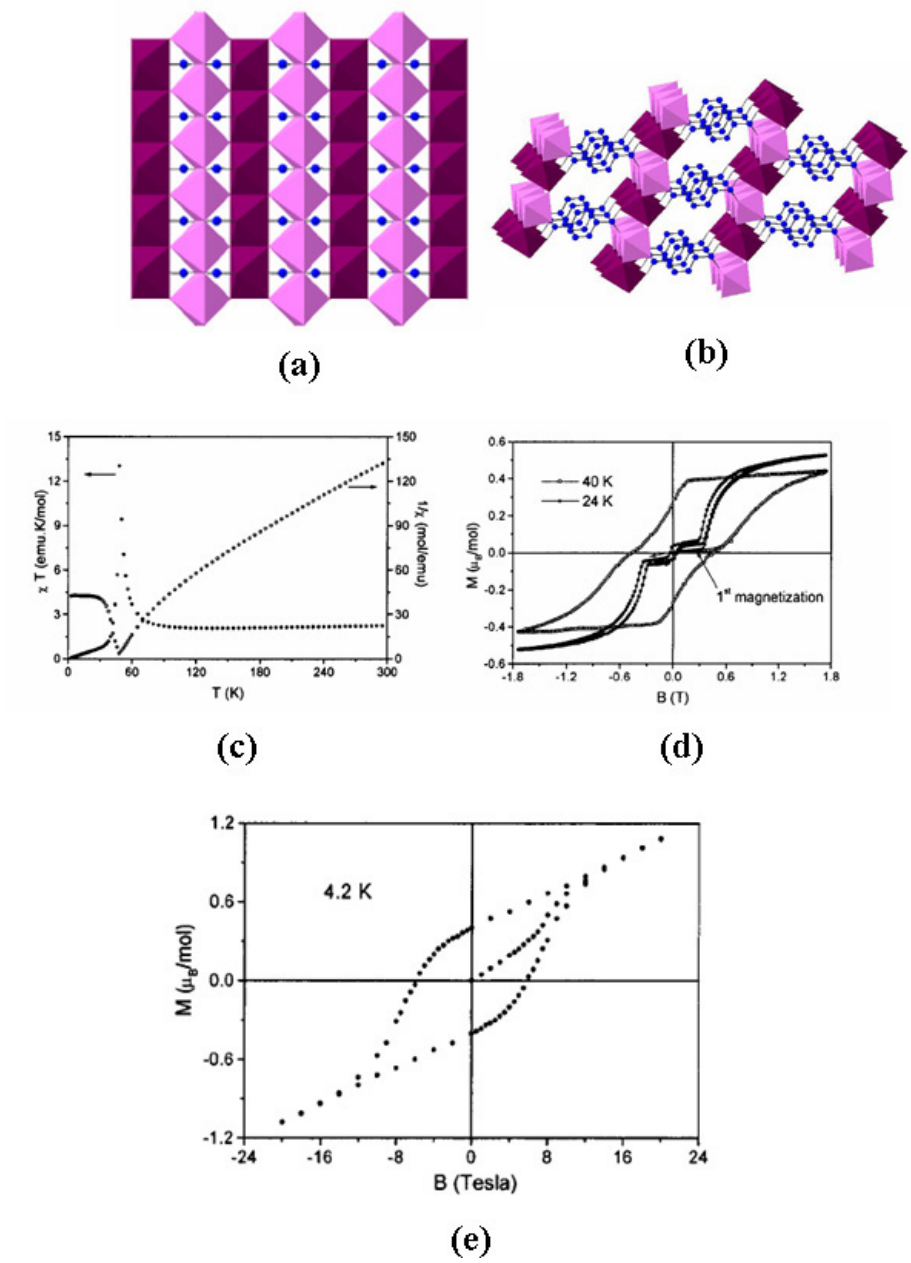

Figure 6. (a) View of the 2D inorganic layer in a 3D cobalt 1,4-benzenedicarboxylate $[Co_2(OH)_2(1,4\text{-BDC})]$, (b) view of the 3D structure where 2D layers are connected by 1,4-BDC anions, (c) temperature dependence of the static χ^{-1} and χT at 50 Oe, (d) field-dependent magnetization at 40, 24 K and (e) high field magnetization up to 20 T at 4.2 K. Reprinted with permission from [46]. Copyright 2000 American Chemical Society.

interactions of the solvent molecules, which not only stabilize the supramolecular structures but also absorb the UV light, preventing the transfer of energy effectively from the ligand to the metal center.

Luminescence from rare earth (RE) based hybrid compounds occurs mainly due to two important processes: (a) emission from the rare earth ion due to direct photoexcitation in the rare earth ion; (b) emission from the rare earth ion due to the fluorescence resonance energy transfer (FRET) from the ligand to the metal center (antenna effect). The efficiency of the emission depends on the rare earth and the degree of the FRET, i.e. energy level comparison between ligand and rare earth. Early work on a very open rare earth glutarate, $[Gd_{1-x}Er_x(glu)]\cdot 4H_2O$, with an I^1O^2 architecture similar to that shown in figure 7, illustrated the potential of this area [61]. The as-synthesized material has water molecules in the channels between the chains, but they can be removed reversibly. It has been shown that the photoluminescent lifetime of the Eu^{3+}-dopant depends upon the degree of dehydration because the coordinating water molecules act as relaxation agents. Such materials clearly have the potential to be used as sensors. In another example, the 3D pyridine-2,5-dicarboxylate, $[Ln_3(OH)_4(2,5\text{-pydc})(2,5\text{-Hpydc})_3(H_2O)_4]$ (Ln = Dy, Eu) exhibits characteristic emissions corresponding to the RE ion. The structure consists of helical dodecahedral chains connected as in a (3, 4) net with I^3Ln–O–Ln connectivity [64].

Table 5. Optical properties of representative inorganic–organic hybrid compounds.

Photoluminescence (PL)					
S. no	Formula	I^nO^m	Origin of PL	Figure	Reference
1	Phthalate $[Cd(1,2\text{-BDC})(H_2O)]$	I^2O^0	π–π^* intraligand fluorescence	—	[58]
2	Oxalate $[Cd_2(C_2O_4)(OH)_2]$	I^2O^1	$\pi^* \rightarrow n$ intraligand transition and LMCT	10	[59]
3	Glutarate $[Gd_{1-x}Er_x(glu)]\cdot 4H_2O$	I^1O^2	Ligand-sensitized metal-centered emission (FRET)	—	[61]
4	Phthalate $[La_{3-x}Ln_x(NO_3)(1,10\text{-phen})_2]$ $[(C_8H_4O_4)4]\cdot H_2O$ (Ln = Tb, Eu)	I^1O^0	Ligand-sensitized metal-centered emission (FRET)	—	[62]
5	Terephthalate $[Ln_3(BDC_{3.5})(OH)_2(H_2O)_2]\cdot H_2O$, Ln = Y:Er–Yb	I^0O^3	FRET and up-conversion	—	[63]

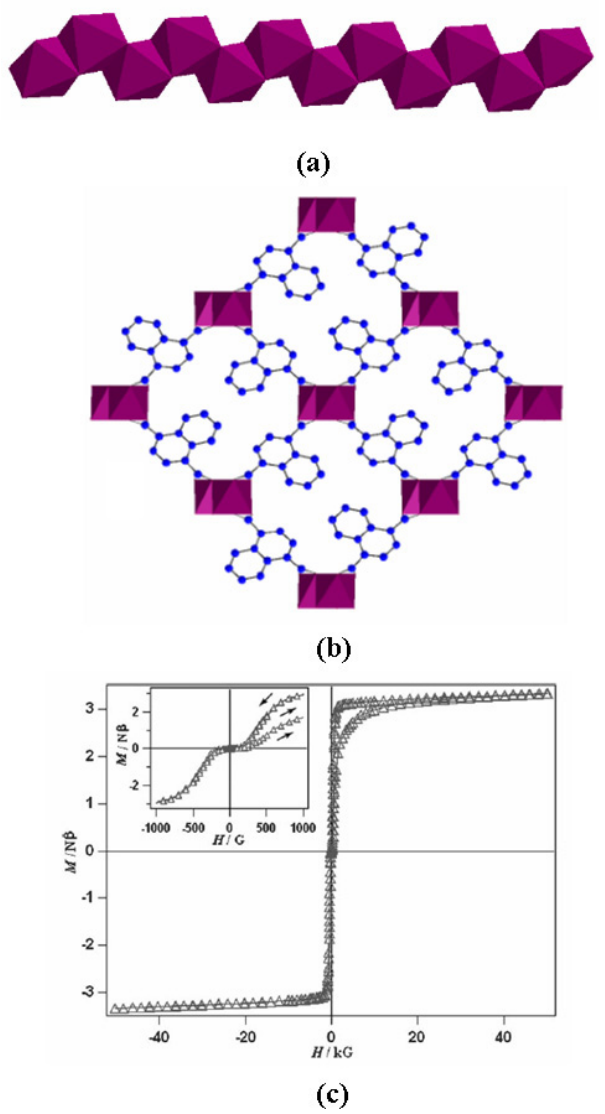

Figure 7. (a) The 1D cobalt oxide chain in 3D 1,4-naphthalenedicarboxylate, [M(1,4-NDC)], M = Co, Mn, (b) view of the 3D structure where 1D chains are connected by 1,4-NDC anions and (c) magnetic hysteresis loop at 2 K (inset: details in a low field showing a sigmoidal curve corresponding to metamagnetic behavior). From [48]. Reproduced by permission of The Royal Society of Chemistry.

A neodymium 1,4-naphthalenedicarboxylate, $[Nd_2(NDC)_3(DMF)_4]\cdot H_2O$, (DMF = *N*,*N*-dimethylformamide), where dinuclears of tricapped trigonal prism are connected into a layered structure by the dicarboxylate ligands, exhibits both PL and up-conversion properties [65]. Under excitation of 488 nm, the compound displays a strong emission band at 1059 nm ($^4F_{3/2} \rightarrow {}^4I_{11/2}$), an emission band at 893 nm ($^4F_{3/2} \rightarrow {}^4I_{9/2}$) with a much lower intensity, and a weak band at 1333 nm ($^4F_{3/2} \rightarrow {}^4I_{13/2}$). A weak UV up-conversion emission at about 391.6 nm and a much stronger blue emission at about 449.5 nm show up upon pulse laser excitation at 580 nm. The intense absorption at 580 nm corresponds to the $^4I_{9/2} \rightarrow {}^4G_{5/2}$ transition, which is a hypersensitive band, satisfying the selection rules of $\Delta J = \pm 2$, $\Delta L = \pm 2$ and $\Delta S = 0$.

5.2. Electroluminescence

Semiconducting luminescent materials would have a filled valence band and an empty conduction band. When an appropriate alternating current (ac) is applied between the two electrodes of a device containing such a material, electron–hole pairs are generated with the possibility of recombination to give emitted light (electroluminescence, EL). The requirements for good EL performance are the ability to transport electrons and holes, and high luminescence efficiency. Hybrid materials, such as semiconducting nanoparticles within an organic polymer matrix or coordination complexes such as $[Ru(bpy)_3]^{2+}$ have been used in EL devices. Strong EL at a low driving voltage was first reported by Tang and Van Slyke in 1987. Thus, the coordination compound, tris(8-hydroxyquinoline)aluminum (Alq_3) has played an important role in light-emitting diodes and has been studied extensively [66]. Tunable emission colors have been obtained by doping other electroluminescent materials into Alq_3, by introducing different substituents into the quinolinolate ligands, or by embedding Alq_3 into mesoporous materials [67].

The use of hybrid inorganic–organic frameworks in EL is relatively new and is receiving attention as materials capable of yielding efficient electroluminescent devices. The well-known 3D Zn_4O(dicarboxylate) (I^0O^3 type), also called MOFs,

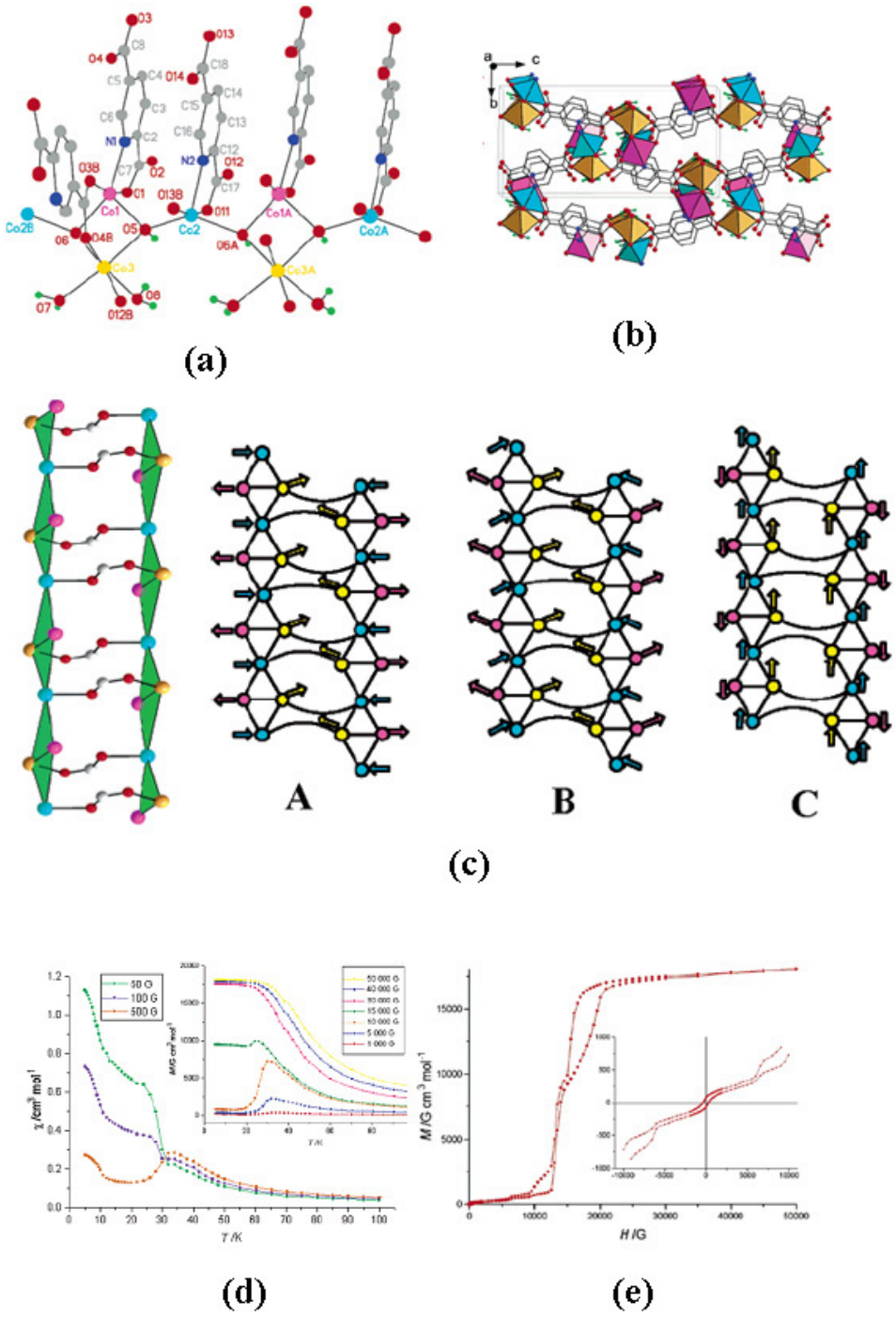

Figure 8. (a) Crystal structure of cobalt 2,5-pyridinedicarboxylate, $[Co_3(NC_5H_3(CO_2)_2)(OH)_2(H_2O)_2]$ showing complete coordination environments of the three Co^{2+} ions, (b) view of the 3D structure, (c) parallel chains of edge- and vertex-sharing triangles with *syn-anti*-carboxylate bridges. Green triangles have μ_3-hydroxide-O at their center (omitted) and suggested arrangement for the spins on the cobalt ions for (A) $H < 10\,000$ G, (B) $10\,000 < H < 15\,000$ G, and (C) $H > 15\,000$ G, (d) plot of χ versus T in small external applied fields, with magnetization data in larger applied external fields (inset) and (e) hysteresis loop for the partially aligned state recorded at 5.0 K, zero field region inset. Reprinted with permission from [50]. Copyright 2004 American Chemical Society.

comprise Zn_4O_{13} units linked by various dicarboxylate ligands. In view of the structural similarities between the zinc clusters in the nodes and semiconductor zinc oxide quantum dots (doped and undoped semiconducting zinc compounds), the MOFs might be expected to exhibit interesting optoelectronic properties. An EL device was made by spreading a uniform film of as-synthesized MOF-5 (zinc 1,4-benzenedicarboxylate) as a wet paste with DMF onto a transparent conductive indium tin oxide (ITO) electrode. From this device, EL emission at about 565 nm was obtained, which is very close to the value of 540 nm found for the corresponding photoluminescence emission maximum. The λ_{EL} (max) obtained for MOF-5 is also

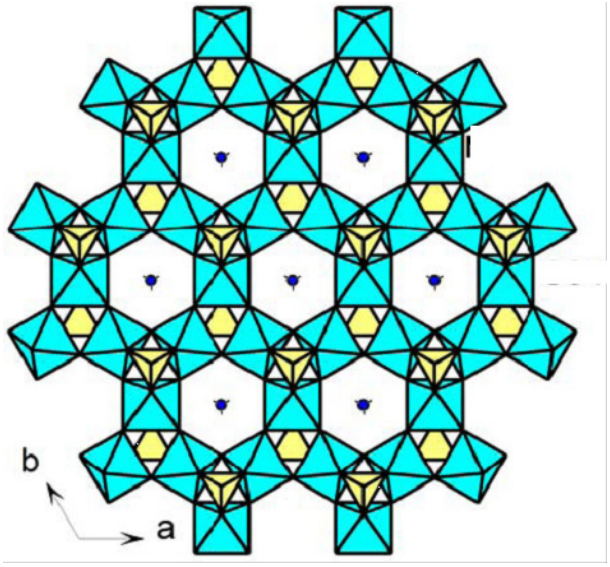

Figure 9. View of the Kagome layer in amine templated $[C_6N_2H_8][NH_4]_2[Ni_3F_6(SO_4)_2]$. Reprinted with permission from [54]. Copyright 2006 American Chemical Society.

very close to the value of 555 nm, which is the wavelength of maximum sensibility of the human eye. By applying an alternating current of 60 V and 180 Hz, a light intensity of 0.4 cd m^{-2} was obtained, which approximately corresponds to an electricity-to-light efficiency conversion of about two lumens W^{-1}. MOF-5 also can be an active component in photovoltaic cells. Similarly, the porosity of MOF frameworks and the possibility of designing them with suitable organic components offer opportunities to have materials with high EL efficiency [68].

5.3. Non-linear optical properties

The availability of novel methods to generate the required asymmetry (both structural as well as electronic asymmetry) in hybrid inorganic–organic compounds, along with their thermal stability and optical transparency, render them to be candidates for nonlinear optical (NLO) materials. Structural asymmetry can be easily generated in hybrid frameworks by using acentric or chiral centers (asymmetric linkers, nodes, polar H-bonds, head-to-tail alignment of dipolar guests confined in channels etc) to create structures with polar or chiral space groups. The use of polarizable ligands and metals with efficient donor–acceptor charge transfer (LMCT or MLCT), or 'hard' and 'soft' ligands trans to one another at the metal center, can ensure electronic asymmetry. Some hybrid materials with NLO properties have been reported (table 6).

Ward and Lin [69, 70] are perhaps the first to develop strategies to engineer non-centrosymmetric frameworks for use as nonlinear optical materials. Here we focus on some recent examples. A powdered sample of 1D $[ZnCl_2(HQA)]\cdot 2.5H_2O$, (HQA = 6-methoxyl-(8S,9R)-cinchonan-9-ol-3-carboxylic acid) shows a strong second harmonic generation (SHG) response of about 20 times larger than that for KDP (KH_2PO_4). Each ligand acts as a bidentate spacer through the nitrogen

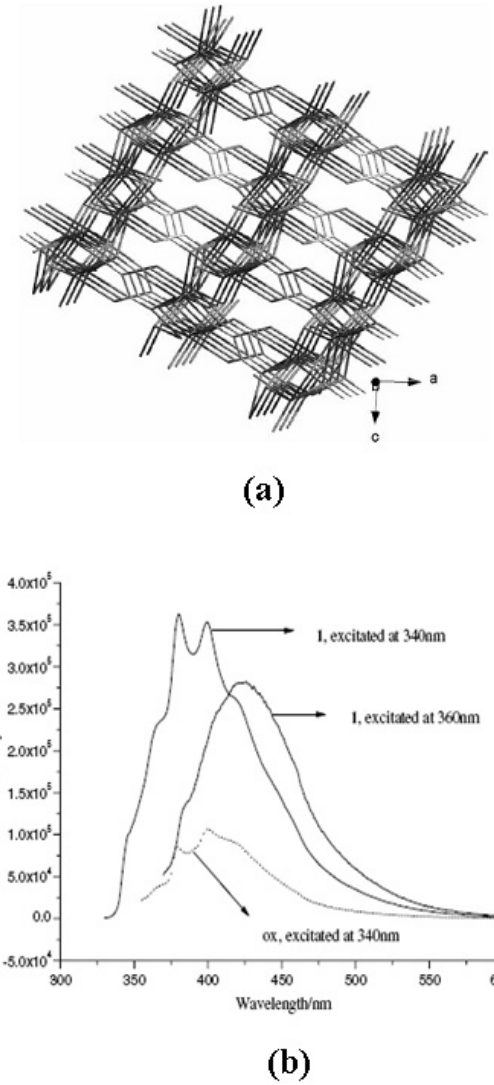

Figure 10. (a) View of the 3D structure of a cadmium oxalate, $[Cd_2(C_2O_4)(OH)_2]$ and (b) fluorescence emission spectra at room temperature for oxalic acid and the compound. Reprinted from [59]. Copyright 2004, with permission from Elsevier.

and carboxylic acid group that links two Zn centers and leads to the formation of a 1D coordination polymer. The compound crystallizes in a chiral space group ($P1$), which belongs to a polar point group ($C1$). Such a strong SHG response was attributed to the presence of intramolecular charge separation due to a zwitterionic moiety generating a large dipole moment ($\mu = qd$, where q is charge and d is distance) (figure 12). A good donor–acceptor chromophore in the ligand was also an essential factor for the observed nonlinear optical behavior [71].

A 3D mixed oxalate–glutarate of neodymium, $Nd_4(H_2O)_2(OOC(CH_2)_3COO)_4(C_2O_4)_2$, comprising a helical column formed by grafting the oxalate unit onto helical NdO_9 chains, cross-linked by the glutarate anions [72], exhibits a frequency-doubled green beam at 532 nm on excitation with a Nd-YAG laser emitting at 1.06 μm. A powdered sample with the homochiral space group $P2_1$ shows about 11 times the SHG activity of KDP. A 3D zinc compound of β-dehydroamino

Table 6. NLO properties of representative inorganic–organic hybrid compounds.

S. no	Formula	I^nO^m	Type of NLO	Figure	Reference
1	$[ZnCl_2(HQA)]\cdot 2.5H_2O$, (HQA = 6-methoxyl-(8S,9R)-cinchonan-9-ol-3-carboxylic acid)	I^0O^1	SHG	12	[71]
2	Oxalate–glutarate $Nd_4(H_2O)_2(OOC(CH_2)_3COO)_4(C_2O_4)_2$	I^1O^2	SHG	—	[72]
3	$[Zn(CN_4–C_6H_4–C_{12}H_7N–C_5H_4N)_2]\cdot 1.5H_2O$	I^0O^3	SHG	13	[74]
4	β-ferrocenylacrylates, $[Pb(OOCCH{=}CHFc)_2(phen)]$ and $[Cd(OOCCH{=}CHFc)_2(H_2O)_2]\cdot(H_2O)_4$	I^0O^3	THG and self-focusing behavior	—	[75]
5	(2,6-dicarboxy-4-hydroxypyridine), $[Zn(C_7H_3O_5N)]\cdot H_2O$	I^0O^2	THG and self-focusing behavior	—	[76]

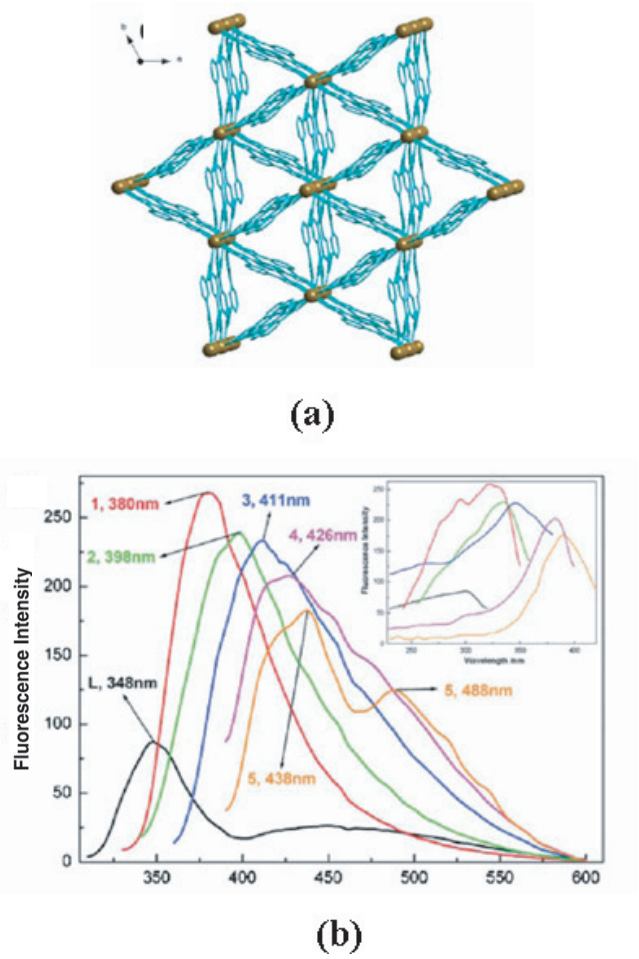

Figure 11. (a) View of the 3D structure $[Cd_3L_6](BF_4)_2$-$(SiF_6)(OH)_2\cdot 13.5H_2O$, ($L$ = 2,6-di-(4-triazolyl)pyridine), without the guest water molecules and anions and (b) luminescence emission spectra at room temperature for ligand (black) and the compound at various degrees of hydration and dehydration (inset shows excitation spectra). From [60]. Reproduced by permission of The Royal Society of Chemistry.

acid, $[Zn\{(E)\text{-}3\text{-}C_5H_4N–C(NH_2){=}CH–COO\}]ClO_4$, obtained from the low symmetry, racemic 3-pyridyl-3-aminopropionic acid [73] crystallizes in a chiral space group ($P2_12_12_1$) and shows a strong SHG response. The presence of the amino group, which is considered to be a good donor, may be expected to enhance the electronic asymmetry (pull–push effect) and advantageous for nonlinear optical behavior.

Two 3D diamond-like networks, $(CN_4–C_6H_5)_2Zn$ and $(NH_2–C_5H_3N–CN_4)_2Zn$ and one two-dimensional square grid network, $[(CN_4–C_6H_4–C_{12}H_7N–C_5H_4N)_2–Zn]\cdot 1.5H_2O$ were crystallized in the non-centrosymmetric space groups $I\text{-}42d$ and $Fdd2$, respectively. The ligands involve a non-center A–D (acceptor–donor) system, a one-center A–D system, and a two-center A–D system, respectively, in those three compounds (figure 13) [74]. All three compounds display strong SHG responses. Among the three complexes, the third one shows the largest SHG effect, which is about 50 and 500 times those of urea and KDP (KH_2PO_4), respectively. The two-center A–D system (multicenter push–pull electronic effect) may be responsible for it having the largest SHG effect.

The 1D β-ferrocenylacrylates, $[Pb(OOCCH{=}CHFc)_2(phen)]$ and $[Cd(OOCCH{=}CHFc)_2(H_2O)_2]\cdot(H_2O)_4$ show third-order NLO properties. Both the chain structures possess infinite 1D M–O–M linkages. The compounds have the same positive sign for the refractive nonlinearity, which gives rise to self-focusing behavior [75]. Their hyperpolarizability (γ) values are calculated to be 5.19×10^{-30} and 1.57×10^{-29} esu for the lead and cadmium compounds, respectively. The γ value of the Cd compound is slightly larger than the Pb compound, which indicates that the metal ions play an important role in the NLO properties of these materials.

A 2D zinc compound of chelidamic acid (2,6-dicarboxy-4-hydroxypyridine), $[Zn(C_7H_3O_5N)]\cdot H_2O$, shows large static third-order polarizability and the convergence value of γ_{xxxx} reaches 6.86×10^{-33} esu in the case of zero input photon energy, which is about three orders of magnitude greater than those of typical organic materials ($\times10^{-36}$ esu). The third-order, nonlinear refractive index value (n_2) was calculated to be 4.15×10^{-11} esu. The structure consists of anticlockwise windmill-like connectivity of metal and ligand with spiroconjugation and an infinitely delocalized π-bond system over the molecular layer [76].

Besides hybrid phosphors, designing materials with other interesting optical properties, especially nonlinear properties, would be of value. Just like one uses a mixture of inorganic phosphors or polymer–inorganic composites, it should be

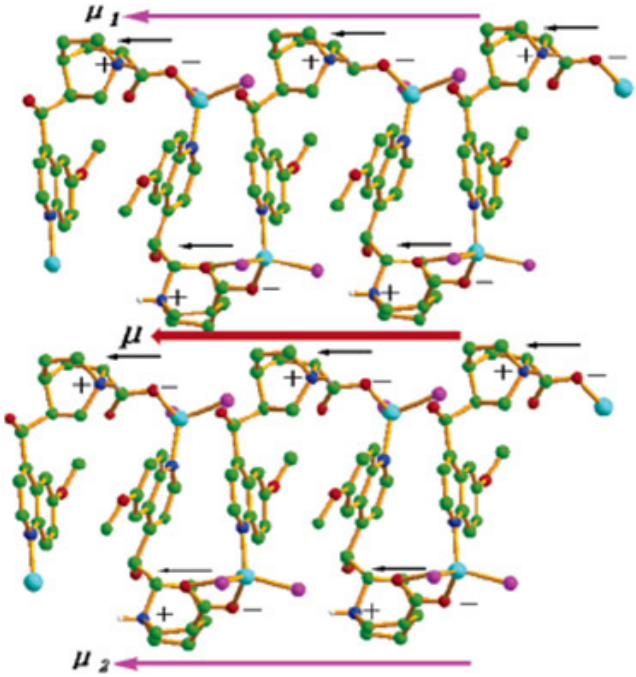

Figure 12. (a) Perspective view of two chains along the *a* axis with the dipolar moment direction in 1D $[ZnCl_2(HQA)]\cdot 2.5H_2O$, (HQA = 6-methoxyl-(8S,9R)-cinchonan-9-ol-3-carboxylic acid). The red arrow is the total dipolar moment ($\boldsymbol{\mu}$), while the purple arrows are the chain dipolar moments $\boldsymbol{\mu}_1$ and $\boldsymbol{\mu}_2$. Reprinted with permission from [71]. Copyright 2006 American Chemical Society.

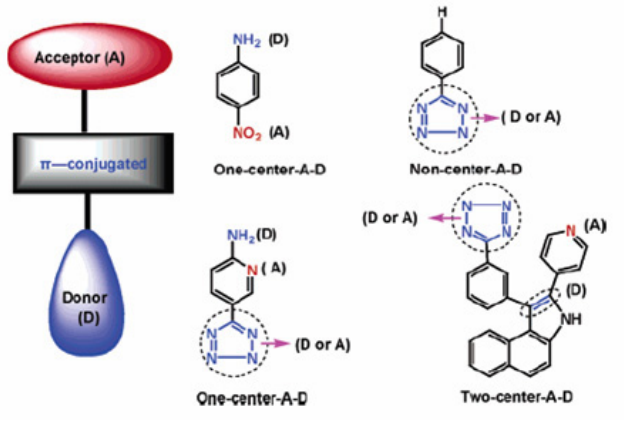

Figure 13. Different types of donor–acceptor systems in various ligands. Reprinted with permission from [74]. Copyright 2005 American Chemical Society.

possible to design hybrids with optical emission properties for potential applications.

6. Electronic properties

Tuning the electronic band structure and thereby controlling the electron-transport properties in hybrid framework compounds has attracted attention because of the availability of various methods for tuning the structure and porosity by a proper selection of donor and acceptor moieties.

The cadmium formate-4,4′-biphenyldicarboxylate, $[Cd_{11}(HCOO)_6(bpdc)_9]\cdot 9DMF\cdot 6H_2O$), has a rare *bcu* topology (I^0O^3 type) in which undecanuclear cadmium clusters are connected by the bpdc units into a 3D structure with large pores. It shows good sorption, optical and semiconducting properties [77]. Photovoltaic (PV) transients can be used to characterize semiconductor materials, and a PV signal will arise whenever light-induced excess charge carriers are separated in space. PV transients at different intensities of the exciting laser pulse (355 nm) were measured (figure 14) and clearly exhibit a time lag caused by the slow and independent diffusion of excess electrons and holes. The times of the PV maxima are similar ($t \approx 0.013$ s) with the different exciting laser pulses (0.05, 0.10, 0.20, and 0.30 mJ). These maxima are related to the separation of charge at the hybrid-ITO interface, and the gradient of excess electron and hole concentrations is caused by the nonhomogeneous absorption of light with photons with $h\nu$ larger than the optical bandgap (E_g). The PV transient signals are positive, which indicates that the photoexcited electrons move faster than holes towards the interface. The maxima of the transients are linearly enhanced when the intensity of the pulse is increased from 0.05 to 0.30 mJ. This observation implies that this compound possesses the characteristics of a diffusion PV transient, but not of a Dember PV transient, which is similar to the case for nanosized metal oxide semiconductors. As mentioned earlier, MOF-5, a terephthalate with quantum dot like Zn_4O_{13} units, also exhibits semiconducting properties, including photocatalysis with reverse shape-selectivity, solar photovoltaic and electroluminescence properties [68].

A 3D compound, $Cu(DCNQI)_2$, (DCNQI = *N*,*N*′-dicyano quinodiimine) formed by the linkages between Cu ion donors and organic DCNQI acceptors exhibits an interesting metal–insulator (M–I) transition under high pressure [78]. This behavior is due to the interaction between the localized 3d-electron bands of the Cu ions and the p-electron conductive bands of DCNQI. Another 1D ribbon, copper-5,6,11,12-tetraazanaphthacene, $[Cu^I(TANC)]$, with alternative metal and ligand shows a high conductivity of 50 S cm^{-1} along the *a* axis at 300 K, but the conductivity sinks rapidly with decreasing temperature, reaching 10^{-6} S cm^{-1} at 10 K [79]. This behavior indicates semiconducting behavior at ambient pressure. Calculations based on the tight-binding approximation yield a 1D energy band and an open Fermi surface. The temperature dependence of the resistivity can be well fitted by the variable-range-hopping (VRH) formula. Application of pressure up to 6.5 GPa increases the purity of the one-dimensionality and the strength of the random potential.

Impedance spectroscopic measurements on a series of novel 3d–4f heterometallic Ln_6Cu_{24} clusters $[Ln_6Cu_{24}(OH)_{30}(Ala)_{12}(Ac)_6(ClO_4)(H_2O)_{12}]\cdot(ClO_4)10\cdot(OH)_7\cdot(H_2O)_{34}$, (Ln = Tb, Gd, Sm and La) with L-alanine as the ligand reveal that they are ionic conductors (figure 15) [80]. The metal skeleton of the cluster may be described as a Ln_6Cu_{12} octahedron (constructed with six Ln^{III} ions located at the vertices and 12 inner Cu^{II} ions located at the midpoints of the edges) connected by 12 additional Cu^{II} ions (every two are connected to one Ln^{III}

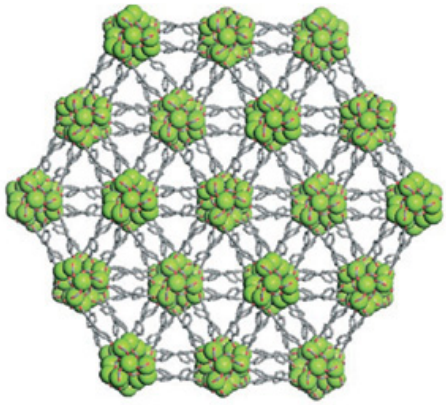

(a)

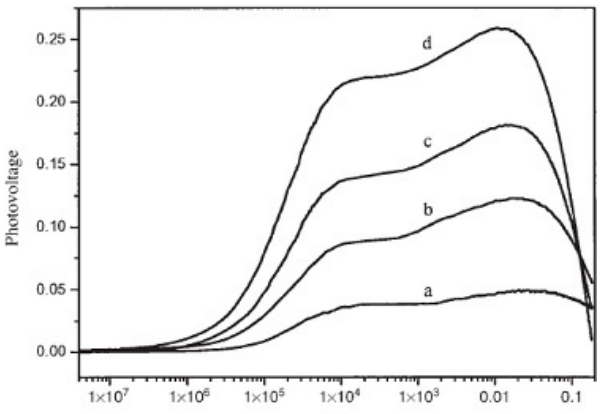

(b)

Figure 14. (a) View of a rare *bcu* topology in 3D cadmium formate-4,4′-biphenyldicarboxylate, $[Cd_{11}(HCOO)_6(bpdc)_9]\cdot 9DMF\cdot 6H_2O$ along the [001] direction and (b) PV transients upon illumination by a 355 nm pulse laser at intensities of *a*—0.05, *b*—0.10, *c*—0.20 and *d*—0.30 mJ. Copyright Wiley-VCH Verlag GmbH & Co. KGaA. Reproduced with permission from [77].

vertex). Conductivity measurements showed typical behavior of an ionic conductor, with a semicircle at high frequencies (from 150 Hz to 300 kHz) and a linear spike at low frequencies (from 20 to 150 Hz). The sample resistance from this plot is 103 K, giving a conductivity of 7.72×10^{-6} S cm^{-1}. The La, Sm and Gd compounds show similar behavior. The sample resistances and conductivities of these complexes are 8.6, 20.2 and 45.8 kΩ and 9.25, 3.94 and 1.74×10^{-5} S cm^{-1}, respectively.

A novel hybrid compound, κ-$BETS_2[Fe^{III}(C_2O_4)Cl_2]$, (BETS = bis(ethylenedithio) tetraselenafulvalene, with both conducting building blocks (π electron) and magnetic molecular building blocks (d electron) in the structure, has been recently reported [81]. The structure consists of parallel donor layers, two per unit cell, displaying a κ type packing of $BETS^{0.5+}$ within the *bc* plane, and anionic magnetic chains, $[Fe(C_2O4)Cl_2]_n^-$, running along the *c* axis (figure 16). It displays metallic behavior down to 4.2 K, with a large optical

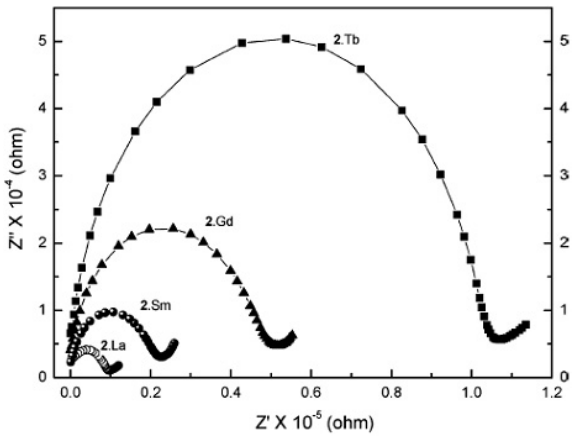

Figure 15. Impedance spectroscopy measurements of the electrical resistance of $[Ln_6Cu_{24}(OH)_{30}(Ala)_{12}(Ac)_6(ClO_4)(H_2O)_{12}]\cdot(ClO_4)10\cdot(OH)_7\cdot(H_2O)_{34}$, at room temperature. Reprinted with permission from [80]. Copyright 2004 American Chemical Society.

anisotropy. The band structure consists of a 1D band and a hole pocket, characteristic of κ phases. The magnetic properties were modeled by the sum of a 1D antiferromagnetic chain contribution from the d spins of Fe^{3+}, a temperature-independent paramagnetic contribution and a Curie impurity term. At 4.5 K, there is a signature of long-range magnetic ordering to a canted antiferromagnetic state in the zero-field-cooled–field-cooled magnetizations, and at 2 K, a small hysteresis loop is observed.

A rather different example of electronic behavior should be mentioned. Kepert and co-workers [82] have discovered an interesting case of spin-crossover in a nanoporous hybrid metal–organic framework compound, $[Fe_2(azpy)_4(NCS)_4\cdot(guest)]$ (azpy is *trans*-4,4′-azopyridine). The crossover is triggered by the uptake or release of molecules into the cavities, providing another example of a sensor system based upon a nanoporous hybrid framework.

Amongst the hybrid materials with novel electronic properties, those which seem feasible are materials which may become superconducting (even at low temperature) and those which exhibit metal–insulator transitions.

7. Dielectrics

It is not surprising that some of the hybrid frameworks exhibit interesting dielectric properties, such as ferroelectricity and other types of ferroic behavior. For example, a 1D chiral $[ZnCl_2(HQA)]\cdot 2.5H_2O$, (HQA = 6-methoxyl-(8S,9R)-cinchonan-9-ol-3-carboxylic acid) shows a dipolar chain relaxation process and a high dielectric constant (ε_0 = 37.3), with a strong SHG response that is about 20 times larger than that for KDP (KH_2PO_4). The properties are attributed to the presence of intramolecular charge separation due to the zwitterionic moiety and a good donor–acceptor chromophore [71].

A 3D $[Cd(papa)(Hpapa)]ClO_4\cdot H_2O$, Hpapa = 3-(3-pyridyl)-3-aminopropionic acid, crystallizes in a non-centric (Cc) polar (C_S) space group. The 3D structure possesses a

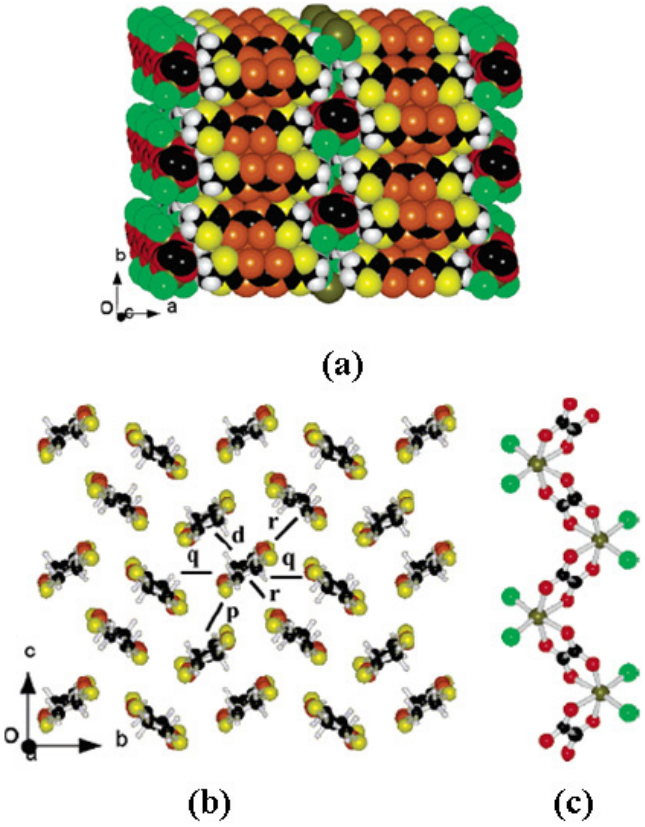

Figure 16. (a) Structure of k-$BETS_2[Fe(C_2O_4)Cl_2]$: a space-filling view of the packing of BETS layers and $[Fe(C_2O4)Cl_2]_n$ chains in the crystal, viewed along the c axis. Color scheme: C, black; H, white; O, red; S, yellow; Cl, green; Fe, brown-green; Se, orange, (b) BETS layer showing the k-type packing of the donors with the definition of the overlap integrals and (c) $[Fe(C_2O4)Cl_2]_n$ chain, viewed along the a axis. Reprinted with permission from [81]. Copyright 2006 American Chemical Society.

novel topology which arises from the connectivity of cadmium ions through a papa unit [73]. This compound exhibits good ferroelectric properties with a dielectric hysteresis loop with a remnant polarization (P_r) of 0.18–0.28 $\mu C\ cm^{-2}$ and coercive field (E_c) of 12 $kV\ cm^{-1}$. The saturation spontaneous polarization (P_s) is about 1.2–1.8 $\mu C\ cm^{-2}$, while those of ferroelectric KDP and triglycine sulfate are 5.0 and 3.0 $\mu C\ cm^{-2}$, respectively.

Another 3D cadmium compound, Cd(TBP)Cl, HTBP = N-(4-(1H-tetrazol-5-yl)benzyl)praline, crystallized in a non-centric (Cc) polar (C_S) space group. This compound exhibits ferroelectric behavior associated with dielectric loss and thus a relaxation process [83]. The electric hysteresis loop shows typical ferroelectric features with a remnant polarization (P_r) of about 0.38 $\mu C\ cm^{-2}$ and coercive field (E_c) of about 2.10 $kV\ cm^{-1}$. Saturation of the spontaneous polarization (P_s) occurs at about 0.50 $\mu C\ cm^{-2}$, which is significantly higher than that for a typical ferroelectric compound (e.g. $NaKC_4H_4O_6{\cdot}4H_2O$, Rochelle salt; usually $P_s = 0.25\ \mu C\ cm^{-2}$). A relaxation process was also observed, suggesting that the dielectric loss changes with temperature at different frequencies with the peak maxima. The relaxation process (peak) is probably associated with dipolar Cd–Cl bond vibrations or the displacement of the proton on the tetrazoyl group in the ligand. It also shows an SHG response of about 10 times that of KDP.

Two multiferroic, homochiral 2D compounds, [Cu((R)-hmp)(dca)] and [Cu((S)-hmp)(dca)], consist of Cu_2O_2 units connected by dicyanamide (dca) and α-methyl-2-pyridinemethanol (hmp) linkers. Both phases show ferroelectric behavior along with a strong antiferromagnetic interaction. They also exhibit an SHG response that is approximately 0.6 times that of urea [84].

Finally, a 3D porous manganese formate, $[Mn_3(HCOO)_6]{\cdot}(C_2H_5OH)$, with 1D channels along the b-axis, exhibits a ferroelectric transition at 165 K and a ferrimagnetic transition at 8.5 K. The compound is a nice example of a hybrid in which the porous host lattice exhibits magnetic order and the behavior of guest molecules can induce ferroelectric behavior. It is also a rare example of a multiferroic system in which ferroelectricity and ferromagnetism co-exist (figure 17) [85].

Besides hybrid materials exhibiting ferroelectricity and related ferroic properties, it would be fascinating to have hybrids which are multiferroic and magnetoelectric. This would require designing materials which are magnetic and are at the same time ferroelectric, preferably with coupling between the electrical and magnetic order parameters.

8. Nanoporous hybrids

Properties of nanoporous hybrid framework solids have been investigated extensively due to their potential applications in catalysis, gas storage, guest exchange, sorption, separation, sensing and other areas [18, 86]. Porous framework solids are conveniently classified into three generations [87, 88]. The first generation compounds have porous frameworks that are often sustained only with guest molecules and the structure may collapse irreversibly on removal of guest molecules. The second generation porous frameworks have stable and robust frameworks, which show permanent porosity without any guest molecules in the pores. The third generation hybrid compounds possess flexible and dynamic frameworks, which respond to external stimuli such as light, electric fields and guest molecules, and are able to change their structure reversibly. The first generation compounds constitute inorganic porous materials constructed by covalent bonds, and include zeolite analogs such as organically templated silicates, phosphates, sulfates etc. The second and third generation compounds are mainly from hybrid inorganic–organic framework solids. In table 7, we list typical examples of porous hybrid materials. In what follows we briefly indicate some of the unusual properties of a few of the porous hybrid framework compounds discovered in recent years.

Most hybrid porous frameworks are coordination polymers of the type I^0O^3. They were realized through crystal engineering by utilizing various geometrical shapes of metal cores (secondary building units (SBUs)) as nodes and multifunctional organic ligands as the linkers. Some of the materials in this class have remarkably large pores and low

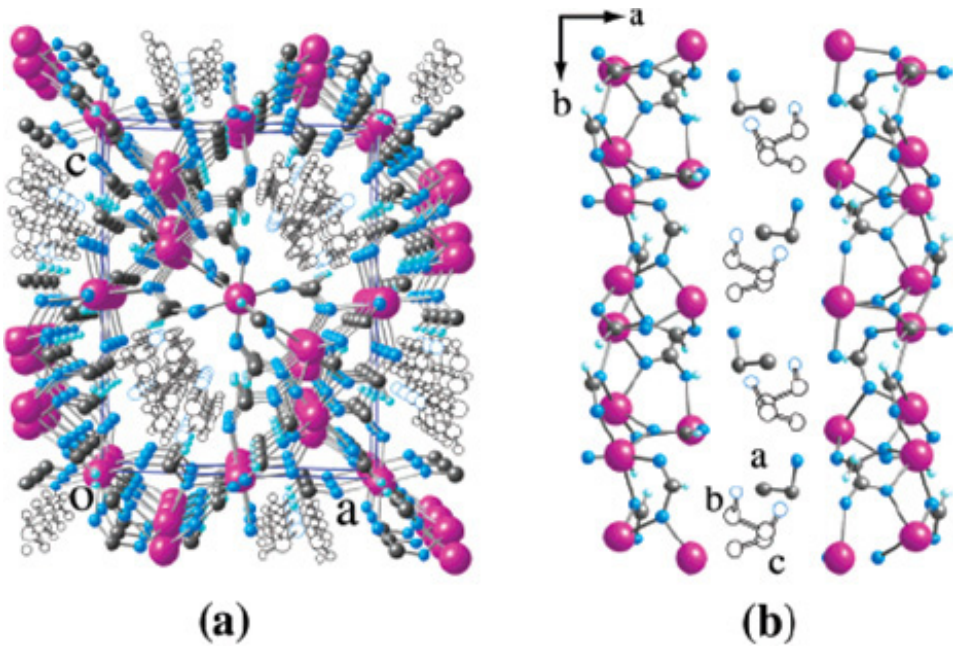

Figure 17. (a) View of the 3D structure of $[Mn_3(HCOO)_6](C_2H_5OH)$ viewed along the *b*-axis: Mn, pink; C, gray; O, blue; H, pale sky blue. The C and O atoms of guest C_2H_5OH molecules are shown by open circles and (b) the arrangement of guest ethanol molecules along the channel at 90 K. Reprinted with permission from [85]. Copyright 2006 American Chemical Society.

densities. For example, a series of MOFs (metal organic frameworks) with high porosity and low densities have been constructed by bridging Zn_4O SBUs via rigid aromatic di- or tricarboxylates [89]. A notable member of the series is MOF-177, $Zn_4O(1,3,5\text{-benzenetribenzoate})_2$, which will store 7.5% hydrogen by weight at 77 K and a pressure of 70 bar [90]. A 3D coordination polymer of the type I^0O^3, the chromium terephthalate, $Cr_3F(H_2O)_2O[(O_2C)\text{-}C_6H_4\text{-}(CO_2)]_3{\cdot}nH_2O$ ($n = 25$) (MIL-101), based on a trinuclear chromium SBU, has an extremely large unit cell (702 000 $Å^3$), very large pore sizes (29–34 Å) and one of the highest internal surface areas reported to date (5900 $m^2\ g^{-1}$) (figure 18) [91]. Some of the porous metal terephthalates (M = Cr and Fe) are being studied for use in drug delivery applications [92].

A 3D lanthanide carboxylate $[Tb(BTB)(H_2O)]\cdot 2(C_6H_{12}O)$, (BTB = 1,3,5-benzenetrisbenzoate), with a I^1O^2 type structure, based upon chains of edge-sharing TbO_9 polyhedra connected by the extended tritopic BTB^{3-} ligand, has 1D hexagonal pores containing free cyclohexanol molecules. When the solvent is removed, this compound with free cylinders of about 10 Å diameter, exhibits a high surface area (>1000 $m^2\ g^{-1}$) [93].

Not all the interesting properties are to be found in systems with large pores. A highly robust 3D erbium 1,4-phenylendiacetate, $[Er_2(PDA)_3(H_2O)]\cdot 2H_2O$ reversibly undergoes dehydration of both coordinated and lattice water molecules to form $[Er_2(PDA)_3]$ of the type I^1O^2. Thermogravimetric analysis shows that $[Er_2(PDA)_3]$ remains stable up to 450 °C [94]. With an effective pore window size of 3.4 Å, it adsorbs CO_2 into its pores and shows nonporous behavior towards Ar or N_2. There is a general correlation between the pore size and the kinetic diameters of the adsorbates (CO_2 = 3.3 Å, Ar = 3.40 Å and N_2 = 3.64 Å). The selectivity of CO_2 over Ar arises from the combined differentiations on size and on host–guest interactions. A 3D 1,3,5-benzenetricarboxylate, $Dy(BTC)(H_2O)\cdot DMF$, with an I^0O^1 type structure and excellent thermal stability (350 °C), shows a high surface area of 655 $m^2\ g^{-1}$ as well as hydrogen and carbon dioxide storage capability due to the availability of Lewis-acid metal sites [95].

Turning to third generations systems, the 3D metal terephthalate, $[M(OH)(OOC\text{–}C_6H_4\text{–}COO)]$, $M = Cr^{III}$, Fe^{III}, Sc^{III}, of the type I^1O^2 exhibits dynamic porosity based on host–guest interactions. This novel dynamic property or the 'breathing effect' occurs when the structure is sufficiently flexible that it can adapt its structure to accommodate sorbates of different sizes and loadings. The structure contains 1D chains of corner-sharing MO_6 octahedra that are cross-linked by the benzene-1,4-dicarboxylate groups to form a 3D network (figure 19). The surface area of the dehydrated form of the Cr(III) member of the MIL-53 family is 1500 $m^2\ g^{-1}$ and it is stable to 500 °C [96]. The dehydrated structure contracts when water is adsorbed due to hydrogen bonding between the water molecules and the oxygen atoms of the benzene-1,4-dicarboxylate groups.

Two 1D coordination polymers, $Ni_2(4,4'\text{-bipyridine})_3(NO_3)_4\cdot 2CH_3OH$ and $Ni_2(4,4'\text{-bipyridine})_3(NO_3)_4\cdot 2C_2H_5OH$, also exhibit dynamic porosity. Both contain linear chains of metal centers bridged by 4,4′-bipyridine, which in turn are connected by further bipy coordination into pairs. These pairs are aligned parallel to each other in the methanol compound and perpendicular in the ethanol system, giving maximum pore cavity dimensions of 8.3 Å with flexible linkers in which the pore openings appear to be too small to allow H_2 to pass. However, they show hysteresis in the adsorption and desorption kinetics above the supercritical temperature of H_2, reflecting the

Table 7. Porous properties of representative inorganic–organic hybrid compounds.

S. No	Formula	I^nO^m	Porous property	Figure	Ref.
1	Zn_4O(1,3,5-benzenetribenzoate)$_2$	I^0O^3	7.5% H_2 storage by weight (77 K, 70 bar)	—	[90]
2	Terephthalate, $Cr_3F(H_2O)_2O$[(1,4-BDC)]$_3\cdot nH_2O$ ($n = 25$)	I^0O^3	Cell dimensions (702 000 Å^3), pore sizes (29–34 Å), surface area (5900 m^2 g^{-1})	18	[91]
3	[Tb(BTB)(H_2O)]$\cdot$2$(C_6H_{12}O)$, (BTB = 1,3,5-benzene trisbenzoate)	I^1O^2	Pore dim. = 10 Å, surface area > 1000 m^2 g^{-1}	—	[93]
4	1,4-phenylendiacetate, $[Er_2(PDA)_3(H_2O)]\cdot 2H_2O$	I^1O^2	Stable up to 450 °C, pore dim. = 3.4 Å, selectivity for CO_2 sorption	—	[94]
5	1,3,5-benzenetricarboxylate, Dy(BTC)$(H_2O)\cdot$DMF	I^0O^1	Stable up to 350 °C, surface area = 655 m^2 g^{-1}, H_2 and CO_2 storage capability	—	[95]
6	Terephthalate, [M(OH)(1,4-BDC)], M = Cr, Fe, Sc	I^1O^2	Stable up to 500 °C, surface area = 1500 m^2 g^{-1}, breathing effect	19	[96]
7	Ni_2(4,4′-bipyridine)$_3$ $(NO_3)_4\cdot$2ROH	I^0O^1	Dynamic porosity, hysteresis in H_2 sorption, pore dim. = 8.3 Å	—	[97]
8	[Ni(bpe)$_2${N(CN)$_2$}]$\cdot$ {N(CN)$_2$}$\cdot 5H_2O$	I^0O^3	Dynamic porosity, anion exchange, selective gas sorption	—	[98]

dynamical opening of the windows between pores. This behavior allows H_2 to be adsorbed at high pressures but stored at lower pressures [97].

Another 3D compound which exhibits dynamic porosity is a bimodal microporous two-fold interpenetrating network of [Ni(bpe)$_2${N(CN)$_2$}]$\cdot${N(CN)$_2$}$\cdot 5H_2O$ (bpe = 1,2-bis(4-pyridyl)ethane; N(CN)$_2$ = dicyanamide). It has two types of channels, one for anionic dicyanamide and the other for neutral water molecules [98]. The dehydrated framework provides a dual function of specific anion exchange of free dicyanamide for the smaller N_3^- anions and selective gas sorption. The N_3^- exchanged framework leads to a dislocation of the mutual positions of the two interpenetrating frameworks, resulting in an increase in the effective pore size in one of the channels and a higher adsorbate capacity than in the initial compound, thereby illustrating the controlled sorption properties of flexible porous frameworks.

Of the various porous hybrid materials that would be of interest, especially important would be materials with high hydrogen uptake. Such materials should have metal sites with little or marginal interaction with hydrogen and possess small or moderate sized pores, surface area not being of great importance. It would be exciting to separate oxygen and nitrogen by passing air through a hybrid material with small magnetic channels.

9. Outlook

The foregoing discussion underlines the wide variety of properties that have already been discovered in hybrid inorganic–organic framework materials, but nevertheless there remains an enormous amount of scope for further work in this area. The number of chemical and structural variations that can be envisaged for hybrid framework compounds is literally infinite, making the scope of this emerging field arguably larger than that of organic and inorganic materials combined. There has been a strong emphasis to date on the study of porous coordination polymers, or MOFs, but, as argued in a recent article [99], there is a great deal of untapped potential in the area of dense materials, many of which have excellent stability. It is also worth remembering that the vast majority of the interesting phenomena studied by physicists are found in dense rather than porous phases.

While some of the physical properties of hybrid materials have been examined, as described in this overview, there is need for greater in-depth studies. Furthermore, there are many properties that are yet to be discovered in hybrid systems, such as thermoelectricity, superconductivity, lasing and metal–insulator transitions. In addition, certain potential combinations of properties may be unique to hybrids. For example, it would be exciting if we could make a hybrid high T_c superconductor with channels into which molecules could be adsorbed. Other unique opportunities may arise from the ease with which homochiral extended solids can be made in this area, opening up the possibility of probing the impact of chirality on other physical properties. Another emerging application of porous hybrids is in catalysis and photochemistry, where host–guest interactions in hybrid frameworks have been exploited to use them as carriers for naked nanoparticles and metal–organic chemical vapor deposition precursors [100–102]. Depositing hybrid compounds on to solid surfaces as thin films for potential

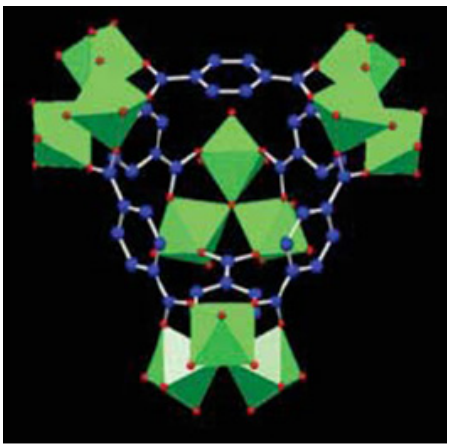

(a)

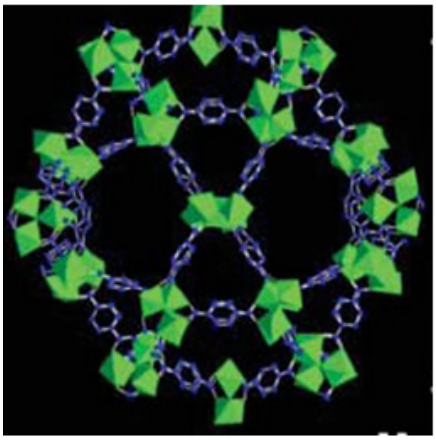

(b)

Figure 18. (a) The super tetrahedron (ST) unit in a 3D chromium terephthalate, $Cr_3F(H_2O)_2O[(O_2C)\text{-}C_6H_4\text{-}(CO_2)]_3{\cdot}nH_2O$ ($n = 25$), where trinuclear chromium SBUs are connected by 1,4-BDC anions and (b) a view of the porous structure built up from the ST units. From [91]. Reprinted with permission from AAAS.

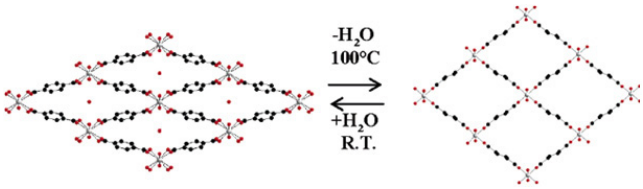

Figure 19. Breathing effect in 3D 1,4-benzenedicarboxylate [M(OH)(OOC–C_6H_4–COO)], M = Cr, Fe, Sc. Copyright Wiley-VCH Verlag GmbH & Co. KGaA. Reproduced with permission from [96].

applications in surface chemistry and physics is also emerging in recent years [103].

There also remains a pressing need for theory and simulation in the hybrid area. One of the challenges lies in predicting the architectures of possible hybrid frameworks and using such predictions to guide synthesis [104]. Other opportunities lie in adapting first principles and force-field methods for the study of hybrids in order to better understand the energetics of such systems [105, 106]. Why, for example, is it so difficult to introduce mixed valency into transition metal hybrids in the quest to discover interesting magnetic and electronic properties? These are some of the many areas where condensed matter physicists will find exciting challenges in this rapidly emerging field.

References

[1] Kitagawa S, Kitaura R and Noro S-i 2004 *Angew. Chem. Int. Edn* **43** 2334
[2] Bailar J C Jr 1964 *Prep. Inorg. React.* **1** 1
[3] Summerville D A, Cape T W, Johnson E D and Basolo F 1978 *Inorg. Chem.* **17** 3297
[4] Miller J S, Vazquez C, Jones N L, McLean R S and Epstein A J 1995 *J. Mater. Chem.* **5** 707
[5] Gravereau P, Garnier E and Hardy A 1979 *Acta Crystallogr.* B **35** 2843
[6] Alberti G, Constantino U, Allulli S and Tomassini N 1978 *Inorg. Nucl. Chem.* **40** 1113
[7] Poojary M D, Hu H-L, Campbell F III and Clearfield A 1993 *Acta Crystallogr.* B **49** 996
[8] Hoskins B F and Robson R 1990 *J. Am. Chem. Soc.* **112** 1546
[9] Robson R 2000 *J. Chem. Soc., Dalton Trans.* 3735
[10] Moulton B and Zaworotko M J 2001 *Chem. Rev.* **101** 1629
[11] Moulton B and Zaworotko M J 2002 *Curr. Opin. Solid State Mater. Sci.* **6** 117
[12] Keeffe M O', Eddaoudi M, Li H, Reineke T and Yaghi O M 2000 *J. Solid State Chem.* **152** 3
[13] Clearfield A 2002 *Curr. Opin. Solid State Mater. Sci.* **6** 495
[14] Cheetham A K and Forster P M 2003 *Top. Catal.* **24** 79
[15] Rowsell J L C and Yaghi O M 2004 *Micropor. Mesopor. Mater.* **73** 3
[16] Rosseinsky M J 2004 *Micropor. Mesopor. Mater.* **73** 15
[17] Rao C N R, Natarajan S and Vaidhayanathan R 2004 *Angew. Chem. Int. Edn* **43** 1466
[18] Cheetham A K, Rao C N R and Feller R K 2006 *Chem. Commun.* 4780
[19] Thirumurugan A, Avinash M B and Rao C N R 2006 *Dalton Trans.* 221
[20] Li H, Eddaoudi M, Keeffe M O' and Yaghi O M 1999 *Nature* **402** 276
[21] Thirumurugan A, Pati S K, Green M A and Natarajan S 2003 *J. Mater. Chem.* **13** 2937
[22] Thirumurugan A and Rao C N R 2005 *J. Mater. Chem.* **15** 3852
[23] Prabhakara Rao K, Thirumurugan A and Rao C N R 2007 *Chem. Eur. J.* **13** 3193
[24] Merrill C A and Cheetham A K 2007 *Inorg. Chem.* **46** 278
[25] Forster P M and Cheetham A K 2002 *Angew. Chem. Int. Edn* **41** 457
[26] Vaidhyanathan R, Natarajan S and Rao C N R 2003 *Dalton Trans.* 1459
[27] Zhang J, Chen S, Valle H, Wong M, Austria C, Cruz M and Bu X 2007 *J. Am. Chem. Soc.* **129** 14168
[28] Bradshaw D, Claridge J B, Cussen E J, Prior T J and Rosseinsky M J 2005 *Acc. Chem. Res.* **38** 273
[29] Byrappa K and Yoshimura M 2001 *Handbook of Hydrothermal Technology: Technology for Crystal Growth and Materials Processing* (Salem, MA: William Andrew Inc.)
[30] Parnham E R and Morris R E 2007 *Acc. Chem. Res.* **40** 1005
[31] Lin Z, Wragg S and Morris R E 2006 *Chem. Commun.* 2021

[32] Forster P M, Burbank A R, Livage C, Férey G and Cheetham A K 2004 *Chem. Commun.* 368
[33] Forster P M, Stock N and Cheetham A K 2005 *Angew. Chem. Int. Edn* **44** 7608
[34] Ni Z and Masel R I 2006 *J. Am. Chem. Soc.* **128** 12394
[35] Jhung S H, Lee J-H, Forster P M, Férey G, Cheetham A K and Chang J-S 2006 *Chem. Eur. J.* **12** 7699
[36] Jhung S H, Jin T, Hwang Y K and Chang J-S 2007 *Chem. Eur. J.* **13** 4410
[37] Jhung S H, Lee J-H, Yoon J W, Serre C, Férey G and Chang J-S 2007 *Adv. Mater.* **19** 121
[38] Guillou N, Livage C, Drillon M and Férey G 2003 *Angew. Chem. Int. Edn* **42** 5314
[39] Kurmoo M, Kumagai H, Hughes S M and Kepert C J 2003 *Inorg. Chem.* **42** 6709
[40] Manna S C, Zangrando E, Bencini A, Benelli C and Chaudhuri N R 2006 *Inorg. Chem.* **45** 9114
[41] Gutschke S O H, Price D J, Powell A K and Wood P T 2001 *Angew. Chem. Int. Edn* **40** 1920
[42] Livage C, Egger C, Noguès M and Férey G 1998 *J. Mater. Chem.* **8** 2743
[43] Livage C, Egger C and Férey G 1999 *Chem. Mater.* **11** 1546
[44] Konar S, Mukherjee P S, Zangrando E, Lloret F and Chaudhuri N R 2002 *Angew. Chem. Int. Edn* **41** 1561
[45] Tong M-L, Wang J and Hu S 2005 *J. Solid State Chem.* **178** 1518
[46] Huang Z-L, Drillon M, Masciocchi N, Sironi A, Zhao J-T, Rabu P and Panissod P 2000 *Chem. Mater.* **12** 2805
[47] Liu P-P, Cheng A-L, Liu N, Sun W-W and Gao E-Q 2007 *Chem. Mater.* **19** 2724
[48] Maji T K, Kaneko W, Ohba M and Kitagawa S 2005 *Chem. Commun.* 4613
[49] Barthelet K, Adil K, Millange F, Serre C, Riou D and Férey G 2003 *J. Mater. Chem.* **13** 2208
[50] Humphrey S M and Wood P T 2004 *J. Am. Chem. Soc.* **126** 13236
[51] Long L-S, Chen X-M, Tong M-L, Sun Z-G, Ren Y-P, Huang R-B and Zheng L-S 2001 *J. Chem. Soc. Dalton Trans.* 2888
[52] Barthelet K, Marrot J, Riou D and Férey G 2002 *Angew. Chem. Int. Edn* **41** 281
[53] Serre C, Millange F, Surblé S, Grenéche J-M and Férey G 2004 *Chem. Mater.* **16** 2706
[54] Behera J N and Rao C N R 2006 *J. Am. Chem. Soc.* **128** 9334
[55] Behera J N and Rao C N R 2007 *Dalton Trans.* 669
[56] Ramirez A P 1994 *Annu. Rev. Mater. Sci.* **24** 453
[57] Pati S K and Rao C N R 2005 *J. Chem. Phys.* **123** 234703
[58] Wang S, Hou Y, Wang E, Li Y, Xu L, Peng J, Liua S and Hua C 2003 *New J. Chem.* **27** 1144
[59] Lu J, Li Y, Zhao K, Xu J-Q, Yu J-H, Li G-H, Zhang X, Bie H-Y and Wang T-G 2004 *Inorg. Chem. Commun.* **7** 1154
[60] Huang Y-Q, Ding B, Song H-B, Zhao B, Ren P, Cheng P, Wang H-G, Liao D-Z and Yan S-P 2006 *Chem. Commun.* 4906
[61] Serpaggi F, Luxbacher T, Cheetham A K and Férey G 1999 *J. Solid State Chem.* **145** 580
[62] Huang Y-G, Wu B-L, Yuan D-Q, Xu Y-Q, Jiang F-L and Hong M-C 2007 *Inorg. Chem.* **46** 1171
[63] Thirumurugan A and Natarajan S 2005 *J. Mater. Chem.* **15** 4588
[64] Yang J, Yue Q, Li G-D, Cao J-J, Li G-H and Chen J-S 2006 *Inorg. Chem.* **45** 2857
[65] Weng D, Zheng X and Jin L 2006 *Eur. J. Inorg. Chem.* **20** 4184
[66] Wang S 2001 *Coord. Chem. Rev.* **215** 79
[67] Huang G S, Wu X L, Xie Y, Kong F, Zhang Z Y, Siu G G and Chu P K 2005 *Appl. Phys. Lett.* **87** 151910
[68] i Xamena F X L, Corma A and Garcia H 2007 *J. Phys. Chem. C* **111** 80
[69] Holman K T, Pivovar A M, Swift J A and Ward M D 2001 *Acc. Chem. Res.* **34** 107
[70] Evans O R and Lin W B 2002 *Acc. Chem. Res.* **35** 511
[71] Tang Y-Z, Huang X-F, Song Y-M, Chan P W H and Xiong R-G 2006 *Inorg. Chem.* **45** 4868
[72] Vaidhyanathan R, Natarajan S and Rao C N R 2004 *J. Solid State Chem.* **177** 1444
[73] Qu Z-R, Zhao H, Wang Y-P, Wang X-S, Ye Q, Li Y-H, Xiong R-G, Abrahams B F, Liu Z-G, Xue Z-L and You X-Z 2004 *Chem. Eur. J.* **10** 53
[74] Ye Q, Li Y-H, Song Y-M, Huang X-F, Xiong R-G and Xue Z 2005 *Inorg. Chem.* **44** 3618
[75] Li L K, Song Y L, Hou H W, Fan Y T and Zhu Y 2005 *Eur. J. Inorg. Chem.* **16** 3238
[76] Zhou G-W, Lan Y-Z, Zheng F-K, Zhang X, Lin M-H, Guo G-C and Huang J-S 2006 *Chem. Phys. Lett.* **426** 341–4
[77] Fang Q-R, Zhu G-S, Jin Z, Xue M, Wei X, Wang D-J and Qiu S-L 2006 *Angew. Chem. Int. Edn* **45** 6126
[78] Kato R 2000 *Bull. Chem. Soc. Japan* **73** 515
[79] Tadokoro M, Yasuzuka S, Nakamura M, Shinoda T, Tatenuma T, Mitsumi M, Ozawa Y, Toriumi K, Yoshino H, Shiomi D, Sato K, Takui T, Mori T and Murata K 2006 *Angew. Chem. Int. Edn* **45** 5144
[80] Zhang J-J, Sheng T-L, Xia S-Q, Leibeling G, Meyer F, Hu S-M, Fu R-B, Xiang S-C and Wu X-T 2004 *Inorg. Chem.* **43** 5472
[81] Zhang B, Wang Z, Zhang Y, Takahashi K, Okano Y, Cui H, Kobayashi H, Inoue K, Kurmoo M, Pratt F L and Zhu D 2006 *Inorg. Chem.* **45** 3275
[82] Halder G J, Kepert C J, Moubaraki B, Murray K S and Cashion J D 2002 *Science* **298** 1762
[83] Ye Q, Song Y-M, Wang G-X, Chen K, Fu D-W, Chan P W H, Zhu J-S, Huang S D and Xiong R-G 2006 *J. Am. Chem. Soc.* **128** 6554
[84] Gu Z-G, Zhou X-H, Jin Y-B, Xiong R-G, Zuo J-L and You X-Z 2007 *Inorg. Chem.* **46** 5462
[85] Cui H, Wang Z, Takahashi K, Okano Y, Kobayashi H and Kobayashi A 2006 *J. Am. Chem. Soc.* **128** 15074
[86] Maspoch D, Ruiz-Molina D and Veciana J 2007 *Chem. Soc. Rev.* **36** 770
[87] Kitagawa S and Kondo M 1998 *Bull. Chem. Soc. Japan* **71** 1739
[88] Kitagawa S and Uemura K 2005 *Chem. Soc. Rev.* **34** 109
[89] W-Foy A G, Matzger A J and Yaghi O M 2006 *J. Am. Chem. Soc.* **128** 3494
[90] Furukawa H, Miller M A and Yaghi O M 2007 *J. Mater. Chem.* **17** 3197
[91] Férey G, Mellot-Draznieks C, Serre C, Millange F, Dutour J, Surblé S and Margiolake I 2005 *Science* **309** 2040
[92] Horcajada P, Serre C, V-Regi M, Sebban M, Taulelle F and Férey G 2006 *Angew. Chem. Int. Edn* **45** 5974
[93] Devic T, Serre C, Audebrand N, Marrot J and Férey G 2005 *J. Am. Chem. Soc.* **127** 12788
[94] Pan L, Adams K M, Hernandez H E, Wang X, Zheng C, Hattori Y and Kaneko K 2003 *J. Am. Chem. Soc.* **125** 3062
[95] Guo X, Zhu G, Li Z, Sun F, Yang Z and Qiu S 2006 *Chem. Commun.* 3172
[96] Loiseau T, Serre C, Huguenard C, Fink G, Taulelle F, Henry M, Bataille T and Férey G 2004 *Chem. Eur. J.* **10** 1373
[97] Zhao X, Xiao B, Fletcher A J, Thomas K M, Bradshaw D and Rosseinsky M J 2004 *Science* **306** 1012
[98] Maji T K, Matsuda R and Kitagawa S 2007 *Nat. Mater.* **6** 142
[99] Cheetham A K and Rao C N R 2007 *Science* **318** 58
[100] Hermes S, Schröter M-K, Schmid R, Khodeir L, Muhler M, Tissler A, Fischer R W and Fischer R A 2005 *Angew. Chem. Int. Edn* **44** 6237

[101] Hermes S, Schröder F, Chelmowski R, Wöll C and Fischer R A 2005 *J. Am. Chem. Soc.* **127** 13744
[102] Shekhah O, Wang H, Strunskus T, Cyganik P, Zacher D, Fischer R and Wöll C 2007 *Langmuir* **23** 7440
[103] Theobald J A, Oxtoby N S, Phillips M A, Champness N R and Beton P H 2003 *Nature* **424** 1029
[104] M-Draznieks C 2007 *J. Mater. Chem.* **17** 4348
[105] Lee C, M-Draznieks C, Slater B, Wu G, Harrison W T A, Rao C N R and Cheetham A K 2006 *Chem. Commun.* 2687
[106] Harvey H G, Slater B and Attfield M P 2004 *Chem. Eur. J.* **10** 3270

J. Phys.: Condens. Matter **20** (2008) 159801 (1pp) doi:10.1088/0953-8984/20/15/159801

Erratum

Hybrid inorganic-organic materials: a new family in condensed matter physics

C N R Rao, A K Cheetham and A Thirumurugan

J. Phys.: Condens. Matter **20** 083202

The authors would like to add the following reference which was forgotten in the list of references:

Guillou N, Livage C, Férey G 2006 *Eur. J. Inorg. Chem.* 4963

The authors would also like to acknowledge the latter authors for their permission to reproduce the coloured versions of figures 2(a),(b), figure 4(a), figures 5(a),(b), figures 6(a),(b) and figures 7(a),(b).

